

文章编号: 0258-7106 (2021) 03-0449-26

Doi: 10.16111/j.0258-7106.2021.03.004

大兴安岭南段毛登矿区阿鲁包格山岩体成岩成矿意义

——锆石、角闪石和黑云母矿物学证据^{*}

季根源^{1,2}, 江思宏^{1**}, 张龙升³, 李高峰^{1,4}, 刘翼飞¹, 易锦俊², 张苏江²

(1 中国地质科学院矿产资源研究所 自然资源部成矿作用与资源评价重点实验室, 北京 100037; 2 自然资源实物
地质资料中心, 河北廊坊 065201; 3 华北地质勘查局综合普查大队, 河北廊坊 065201;
4 北京大学造山带与地壳演化重点实验室, 北京 100871)

摘要 毛登矿区位于内蒙古锡林浩特, 是大兴安岭南段典型的锡钼铋多金属矿床。文章选择毛登矿区阿鲁包格山斑状二长花岗岩为研究对象, 开展了高精度锆石 U-Pb 定年和锆石、角闪石、黑云母矿物学研究, 以探讨成岩时代、岩浆结晶的物理化学条件及其对成矿的意义。结果显示, 斑状二长花岗岩锆石 U-Pb 年龄(140 ± 0.9)Ma, 侵位于早白垩世; 锆石 $w(\text{Ti})$ 为 $(3.99 \sim 10.9) \times 10^{-6}$, 结晶温度 $672 \sim 805^\circ\text{C}$ (平均 734°C), 岩浆氧逸度 $\lg f(\text{O}_2)$ 为 $-19.6 \sim -14.4$ 。角闪石化学成分显示富铁($w(\text{TiFeO})$ 为 $22.38\% \sim 26.41\%$)、富钙($w(\text{CaO})$ 为 $9.57\% \sim 10.36\%$)、贫镁($w(\text{MgO})$ 为 $5.67\% \sim 8.09\%$), 暗示了岩浆经历了明显的结晶分异演化作用; $w(\text{Al}_2\text{O}_3)$ 为 $5.13\% \sim 6.29\%$, 小于 10% , 以及 $\text{Si}/(\text{Si}+\text{Ti}+\text{Al})$ 值($0.86 \sim 0.88$)大于 0.765 , 表明具壳源角闪石特征; 角闪石结晶温度 $709 \sim 753^\circ\text{C}$, 形成压力 $145 \sim 241 \text{ MPa}$, 形成深度 $5.5 \sim 9.1 \text{ km}$, 寄主岩浆氧逸度 $\lg f(\text{O}_2)$ 为 $-16.6 \sim -15.4$, 含水量 $\text{H}_2\text{O}_{\text{melt}}$ 为 $3.6\% \sim 4.4\%$ 。黑云母化学成分显示, 富铁($w(\text{TiFeO})$ 为 $24.73\% \sim 28.53\%$)、镁($w(\text{MgO})$ 为 $6.21\% \sim 9.02\%$), $I_{\text{Mg}}(\text{Mg}/(\text{Fe}+\text{Mg}))$ 值($0.28 \sim 0.39$)小于 0.5 , 表明具壳源黑云母特征; 黑云母结晶温度为 $650 \sim 712^\circ\text{C}$, 寄主岩浆氧逸度 $\lg f(\text{O}_2)$ 为 $-18.3 \sim -16.5$; 黑云母 I_{Mg} 值与华南含锡花岗岩 I_{Mg} 值区间范围一致, 且 I_{Fe} 值($0.61 \sim 0.72$)较高, 显示岩体与矿区 Sn 矿化关系密切。结合前人研究, 认为斑状二长花岗岩可能为新生地壳经部分熔融后, 在上升过程中经历较明显的结晶分异演化作用而形成; 具 A 型花岗岩特征, 成岩环境处于伸展构造背景。岩浆演化处于较低氧逸度, 较高温度, 较高的水、F 和 Cl 含量的环境, 是毛登矿区锡、钼、铋多金属矿化形成的重要条件。

关键词 地球化学; 锆石; 角闪石; 黑云母; 大兴安岭南段; 毛登矿床

中图分类号:P618.44; P618.65; P618.69

文献标志码:A

Petrogenic and metallogenic significance of Alubaogeshan granite in Maodeng deposit of southern Da Hinggan Mountains: Evidence from mineralogy of zircon, amphibole and biotite

JI GenYuan^{1,2}, JIANG SiHong¹, ZHANG LongSheng³, LI GaoFeng^{1,4}, LIU YiFei¹,
YI JinJun² and ZHANG SuJiang²

(1 MNR Key Laboratory of Metallogeny and Mineral Assessment, Institute of Mineral Resources, CAGS, Beijing 100037, China;
2 Cores and Samples Center of Natural Resources, Langfang 065201, Hebei, China; 3 Exploration Unit of North China Geological
Exploration Bureau, Langfang 065201, Hebei, China; 4 Key Laboratory of Orogen and Crust Evolution,
Peking University, Beijing 100871, China)

* 本文得到国家自然科学基金项目(编号: 41873051)、科技部深地项目(编号 2017YFC0601303)和地质调查项目(编号 DD20190411、
DD20201113)联合资助

第一作者简介 季根源, 男, 1987 年生, 工程师, 博士研究生, 矿物学、岩石学、矿床学专业。Email: csujigenyuan@163.com

** 通讯作者 江思宏, 男, 1968 年生, 研究员, 博士, 博士生导师, 主要从事金属矿床成矿规律研究。Email: jiangsihong1@163.com

收稿日期 2021-01-10; 改回日期 2021-04-22。秦思婷编辑。

Abstract

Located in Xilin Hot City of Inner Mongolia, the Maodeng deposit is a typical Sn-Mo-Bi polymetallic deposit in the southern segment of Da Hinggan Mountains. In this paper, the authors present high-precision zircon U-Pb ages as well as chemical compositions of zircon, amphibole and biotite from Alubaogeshan porphyritic monzogranite in the Maodeng deposit, aiming to investigate the petrogenic age, the formation conditions and the petrogenic and metallogenetic significance of this rock body. The zircon yielded a weighted mean U-Pb age of (140 ± 0.9) Ma, which indicates that the emplacement of porphyritic monzogranite took place during the Early Cretaceous. Ti content of zircon ranges from 3.99×10^{-6} to 10.9×10^{-6} and crystallization temperature of zircon is $672\text{--}805^\circ\text{C}$ with an average of 734°C . The oxygen fugacity $\lg f(\text{O}_2)$ of the magma was $-19.6\text{--}-14.4$ when zircon crystallized. Electron microprobe analyzer (EMPA) analysis shows that the amphibole is rich in iron ($w(\text{TFeO})=22.38\%\text{--}26.41\%$) and calcium ($w(\text{CaO})=9.57\%\text{--}10.36\%$) but poor in magnesium ($w(\text{MgO})=5.67\%\text{--}8.09\%$), which indicates that the magma has experienced obvious evolution. The content of Al_2O_3 ($5.13\%\text{--}6.29\%$) is lower than 10%, whereas the $w(\text{Si})/w(\text{Si+Ti+Al})$ ratio ($0.86\text{--}0.88$) is higher than 0.765, indicating that the amphibole was derived from the crust. The crystallization temperature of amphibole is $709\text{--}753^\circ\text{C}$, with the crystallization pressure of $145\text{--}241$ MPa and the emplacement depth of $5.5\text{--}9.1$ km. The oxygen fugacity $\lg f(\text{O}_2)$ of magma was $-16.6\text{--}-15.4$, and the water content ($\text{H}_2\text{O}_{\text{melt}}$) was $3.6\%\text{--}4.4\%$ when the amphibole crystallized. The biotite is rich in iron ($w(\text{TFeO})=24.73\%\text{--}28.53\%$) but poor in magnesium ($w(\text{MgO})=6.21\%\text{--}9.02\%$). The $I_{\text{Mg}}(\text{Mg}/(\text{Fe+Mg}))$ values change from 0.28 to 0.39, suggesting that the biotite is crustal. The oxygen fugacity $\lg f(\text{O}_2)$ of magma was $-18.3\text{--}-16.5$ and the temperature was $650\text{--}712^\circ\text{C}$ when biotite crystallized. The I_{Mg} value is consistent with that of tin-bearing granite in South China, and the $I_{\text{Fe}}(\text{Fe}/(\text{Fe+Mg}))$ value ($0.61\text{--}0.72$) is relatively high. It is believed that the porphyritic monzogranite is related to the Sn mineralization in the Maodeng deposit. In combination with previous studies, the authors hold that the porphyritic monzogranite was dominantly derived from the partial melting of a juvenile lower crust, followed by strong fractional crystallization during magma ascent. The porphyritic monzogranite belongs to A-type granite, which was formed in an extensional setting. The magma has relatively high H_2O , F and Cl content, suggesting that it evolved under the condition of relatively low oxygen fugacity, high temperature and shallow emplacement. Therefore, it is believed that the porphyritic monzogranite played an important role in Sn-Mo-Bi polymetallic mineralization in the Maodeng deposit.

Keywords: geochemistry, zircon, amphibole, biotite, southern segment of Da Hinggan Mountains, Maodeng deposit

大兴安岭南段广泛发育与高度演化的花岗岩关系密切的W、Sn、Ag、Mo、Pb、Zn、稀土、稀有等金属矿床,如白音查干Sn-Ag-Cu-Pb-Zn矿床(姚磊等,2018;李睿华,2019)、维拉斯托Sn-Cu-Pb-Zn-Ag-Li-Rb-Nb-Ta矿床(刘瑞麟等,2018;Liu et al., 2016; Wang et al., 2017)、黄岗Sn-Fe-Pb-Cu矿床(周振华等,2010;翟德高等,2012)、巴尔哲REE-Nb-Be-Zr矿床(王一先等,1997)、敖仓花Mo-Cu矿床(马星华等,2009)、半砬山钼矿床(Zhang et al., 2010; Shu et al., 2016)、毛登Sn-Mo-Bi矿床(石得凤,2007;张巧梅等,2013)等,逐渐成为中国北方地区重要的钨、锡、钼、银、铅、锌、稀土和稀有矿产基地。大兴安岭南段

先后经历了古亚洲洋的闭合、古太平洋和蒙古-鄂霍茨克洋板块俯冲等复杂的构造历史,发育大规模不同时代、不同类型的花岗岩,区内多金属矿床主要与早白垩世高度演化的花岗质岩体有密切关系(Engebretson et al., 1985;赵一鸣等,1997;毛景文等,2013;江思宏等,2018)。因此,前人对区内早白垩世花岗质岩体开展了大量的研究,包括成岩年代学、岩石地球化学、同位素地球化学以及成岩构造背景等(郭锋等,2001;Fan et al., 2003;王京彬等,2005;王长明等,2006;邵济安等,2010;Ouyang et al., 2015;Liu et al., 2016;Zhai et al., 2017),但对高度演化的花岗岩浆演化过程中的矿物学特征以及物理化学条件研究较为

薄弱甚至缺乏,这在一定程度上制约了花岗岩成岩作用精细刻画以及对成矿意义的评价。

前人研究表明,花岗岩结晶时的温压、氧逸度、挥发分含量、含水量等物理化学条件对W、Sn、Cu、Au、Pb、Zn、Ag、Mo等金属成矿元素在熔体和流体相之间运移、分配,以及成岩、成矿作用或两者成因关系具有重要的影响(李鸿莉等,2007;张德会,2015)。岩石的矿物成分和组合是岩浆原始成分的直接反映。锆石是花岗岩中广泛发育的副矿物之一,不易受热液蚀变、变质作用和表生作用的影响,常被用作记录岩浆原始信息的载体矿物,广泛应用于年代学和岩石成因及演化研究中(Hoskin et al., 2000; Ballard et al., 2002; Belousova et al., 2006; Ferry et al., 2007; Li et al., 2019)。黑云母和角闪石是花岗岩中重要的造岩矿物,其化学成分特征能够反映花岗岩结晶时的物理化学条件、岩浆演化特征,以及岩浆源区的性质和构造环境等重要信息(Wones et al., 1965; 姜常义等, 1984; Hammarstrom et al., 1986; Abdel-Rahman, 1994; Henry et al., 2005; Ridolfi et al., 2008; 2010; Hossin et al., 2014; Brisken et al., 2015),因而对深入研究和认识花岗岩的形成和演化具有重要的指示作用。

毛登矿床位于内蒙古锡林浩特市北东约50 km处,是大兴安岭南段与岩浆热液作用有关的典型锡钼铋多金属矿床(刘玉强 1996a; 1996b; 张巧梅等, 2013)。前人研究显示,矿区东部阿鲁包格山复式岩体与成矿关系密切,该岩体主要为斑状二长花岗岩,边缘过渡为花岗斑岩和碱长花岗岩(程天赦等, 2014; 郭硕等, 2019; 李睿华, 2019)。在详细野外地质调查工作的基础上,本文选择毛登矿区斑状二长花岗岩体中锆石、黑云母和角闪石作为研究对象,开展详细的岩相学、锆石年代学、矿物学研究,限定成岩过程的物理化学条件,探讨岩体成因与演化及其对成矿的制约,同时揭示岩体源区特征及形成构造背景,为进一步认识大兴安岭南段地区燕山晚期岩浆演化及与之关系密切的金属成矿作用提供参考依据。

1 矿区与矿床地质

毛登矿区地处大兴安岭南段西坡锡林浩特-锡林郭勒 Sn-Ag-Cu-Pb-Zn-Mo 成矿亚带(图 1a),位于古亚洲洋、古太平洋和蒙古-鄂霍茨克洋构造体系叠加区域。蒙古-鄂霍茨克洋造山后伸展和古太平洋

俯冲的联合作用下强烈的构造-岩浆活动是区域上形成巨型成矿域的重要原因(赵一鸣等, 1997; 刘建明等, 2004; 江思宏等, 2018; Engebretson et al., 1985; Ouyang et al., 2015)。区域内主要出露的地层包括下二叠统寿山沟组砂岩、粉砂岩、杂砂岩和砾岩;下二叠统大石寨组凝灰质粉砂岩、细砂岩、流纹岩、火山角砾岩、安山岩、凝灰岩和玄武岩;下侏罗统红旗组砂岩、砂砾岩以及泥岩;上侏罗统玛尼土组中酸性火山熔岩、火山碎屑岩;下白垩统白音高老组流纹岩、火山角砾岩、凝灰岩(图 1b)。其中,大石寨组酸性-中性-基性火山岩-火山碎屑岩组合以及陆源碎屑沉积岩是区内多金属矿床的主要赋矿地层。区域内断裂构造较发育,海西晚期发育北东向逆冲断层和正断层以及北西向平移断裂,北东向断裂为燕山期花岗岩体的侵位提供了通道,燕山期发育北东向和北西向断裂,北东向与北西向断裂交汇处为重要的容矿构造。区域内燕山期阿鲁包格山复式岩体出露于毛登矿区东部,面积约 49 km²,呈近等轴状岩株产出,无明显定向延伸,与大石寨组、白音高老组和红旗组呈侵入接触关系(图 1b)。

毛登矿床位于阿鲁包格山岩体西缘,在 20 世纪,锡和铜探明储量为中型规模,近年来,深部地质勘查工作显示出新探明钼和铋资源量分别突破 16 万 t 和 10 万 t,均达大型规模(河南省有色金属地质勘查总院,2009)。毛登矿床出露地层有下二叠统大石寨组、下侏罗统红旗组、下白垩统白音高老组以及第四系,大石寨组岩性主要为火山角砾岩、含火山角砾熔岩和变质粉砂岩等,是矿区内的赋矿围岩(图 2)。矿区内的北西向断裂及节理、裂隙是区内主要容矿构造。矿区东侧见阿鲁包格山复式岩体,以斑状二长花岗岩为主,花岗斑岩侵位于岩体边缘部位(图 1b),碱长花岗岩侵位于矿床深部(图 3),3 种不同岩性相呈渐变关系,无明显界线,与锡钼铋多金属矿化关系联系紧密(程天赦等,2014; 郭硕等,2019; 李睿华,2019)。

矿床上部发育 Sn-Cu 矿体,下部发育 Mo-Bi 矿体(图 3)。Sn-Cu 矿体以石英脉状赋存于岩体外接触带大石寨组火山角砾岩,次为花岗斑岩体和变质粉砂岩中;矿体受北西向断裂-裂隙控制,呈陡倾斜平行密集脉状产出;金属矿物主要有锡石、黄铜矿、闪锌矿、毒砂、斑铜矿、黄铁矿、黑钨矿、辉钼矿,少量的黝铜矿、方铅矿、黄锡矿、磁黄铁矿、硫锑铅矿等;非金属矿物主要有黄玉、绢云母、白云母、石英、萤石,少量的独居石、板钛矿等(刘玉强, 1996a; 1996b;

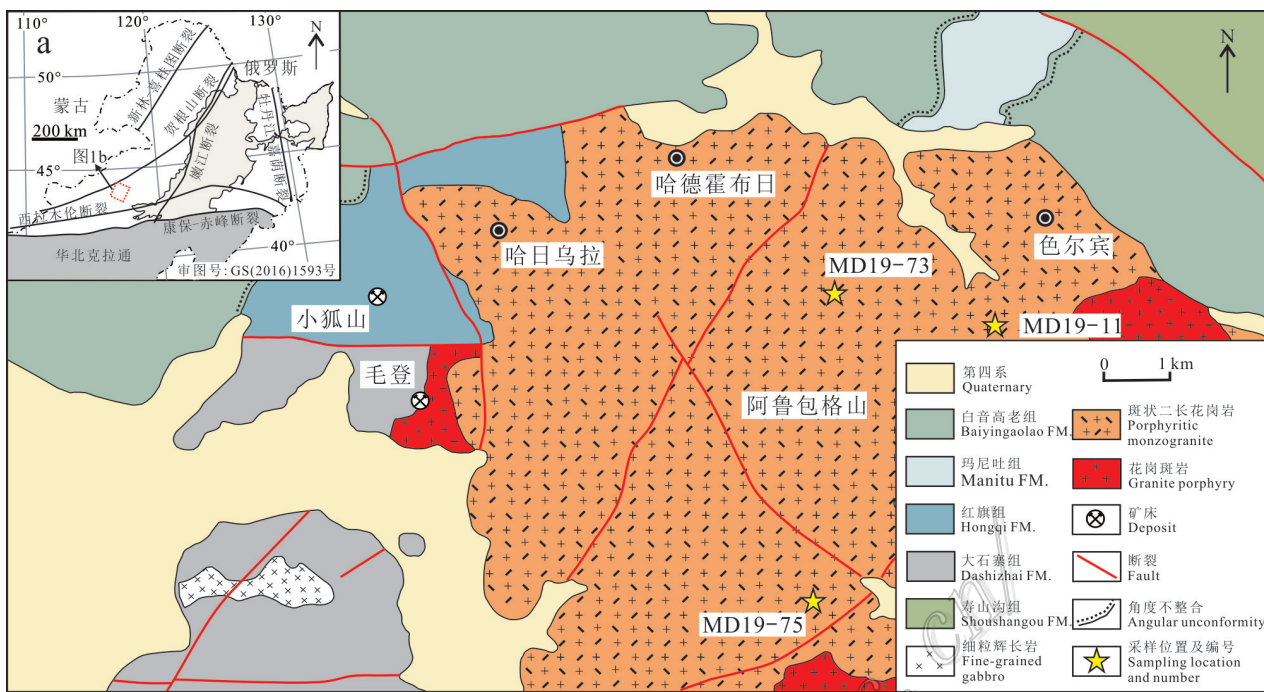


图1 毛登矿区大地构造位置图(a, 修改自Chen et al., 2017)和区域地质简图(b, 修改自张学斌等, 2014; 郭硕等, 2019)

Fig. 1 Sketch map showing the location of the Maodeng deposit (a, modified after Chen et al., 2017) and regional geological

sketch map of the Maodeng deposit (b, modified after Zhang et al., 2014; Guo et al., 2019)

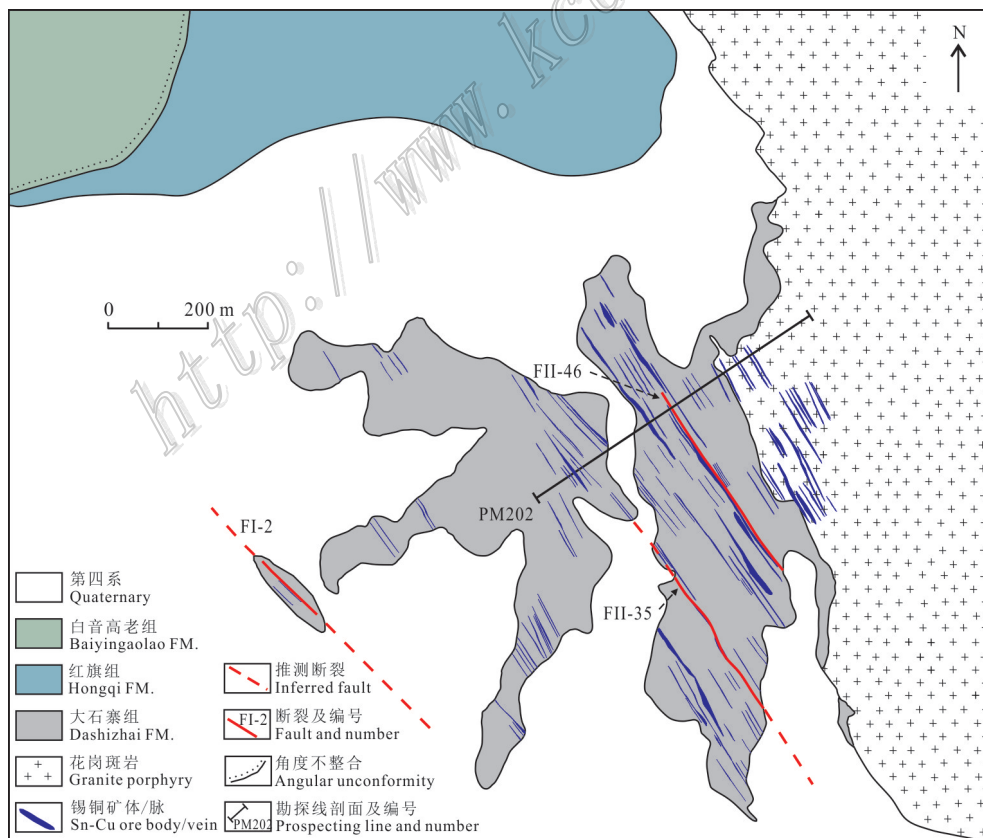


图2 毛登矿床地质简图(修改自石得凤, 2007; 张巧梅等, 2013; 郭硕等, 2019)

Fig. 2 Geological sketch map of the Maodeng deposit (modified after Shi, 2007; Zhang et al., 2013; Guo et al., 2019)

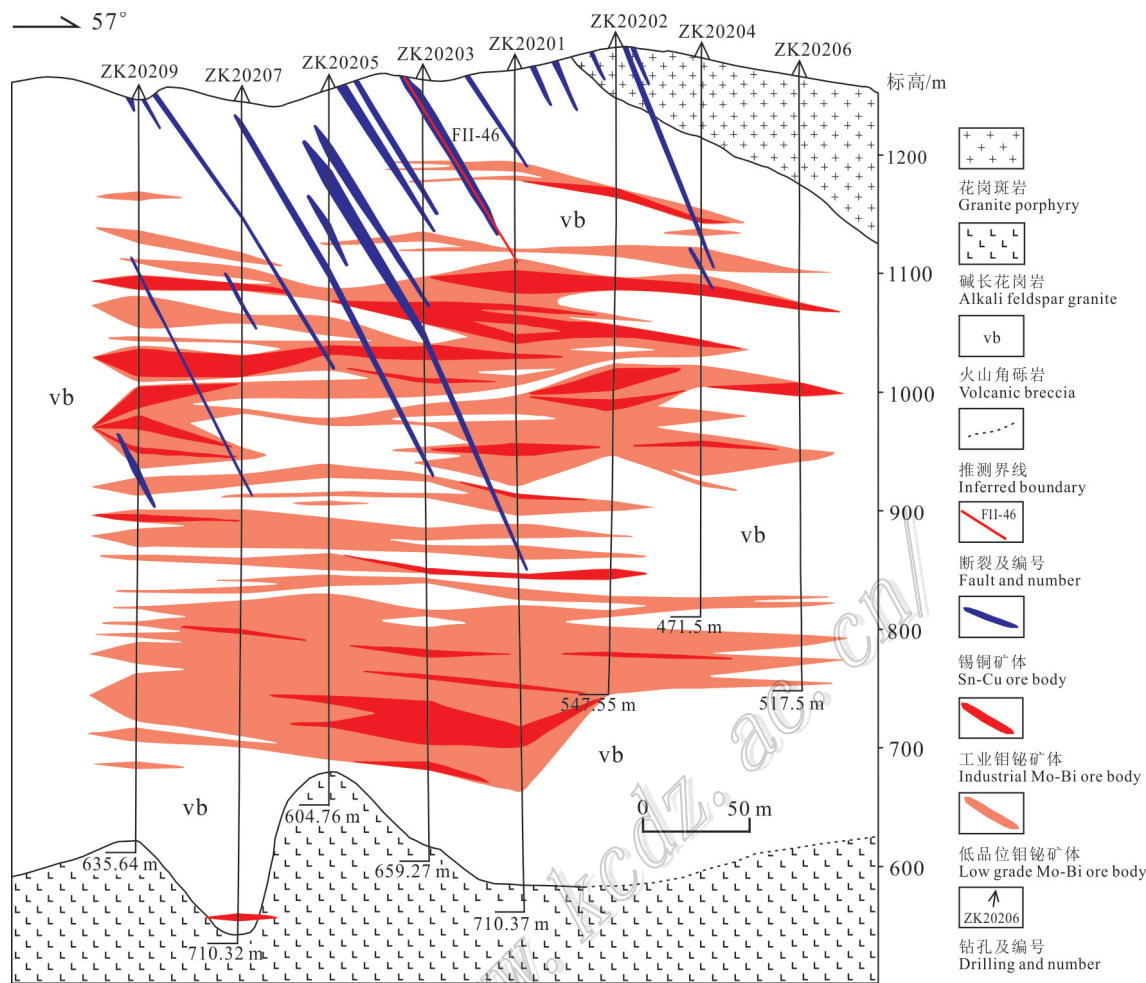


图3 毛登矿床202号勘探线剖面图(修改自河南省有色金属地质勘查总院,2009)

Fig. 3 Geological section along No. 202 exploration line in the Maodeng deposit (modified after Henan Provincial Non-ferrous Metal Geological Exploration General Institute, 2019)

石得凤,2007;张巧梅等,2013)。Mo-Bi矿体以网脉状、微-细脉状和浸染状赋存于岩体外接触带大石寨组火山角砾岩和变质粉砂岩中;在岩浆侵入或岩体上拱后的应力作用下,上覆地层火山角砾岩、变质粉砂岩发育密集节理、裂隙微构造,是主要的赋矿、控矿构造;金属矿物主要有辉钼矿、自然铋,少量的毒砂、黄铜矿、方铅矿、闪锌矿、黄铁矿等;非金属矿物主要有石英、绢云母,少量萤石、黄玉、维晶黑云母、残留斜长石和钾长石、方解石等。

2 样品采集与分析方法

本次研究的样品均采自毛登矿区阿鲁包格山花岗岩体的地表露头。样品MD19-11(E116°41'11", N44°11'18")、MD19-73(E116°39'16.5", N44°

11'39")、MD19-75(E116°39'7", N44°8'50")分别采自岩体东部、东北部和南部(图1b),均为新鲜的斑状二长花岗岩。镜下观察发现,斑状二长花岗岩具似斑状结构-基质细粒花岗结构,块状构造(图4)。斑晶由斜长石(含量20%~30%)、钾长石(含量30%~40%)、石英(含量10%~15%),以及角闪石(含量1%~5%)和黑云母(少量)暗色矿物构成,杂乱分布,粒径一般2~15 mm,部分0.5~2.0 mm。斜长石,呈半自形板状结构,环带不明显,聚片双晶清晰,表面较干净,弱高岭土化、绢云母化;钾长石,呈半自形板状结构,经鉴定为正长石,轻微高岭土化,内见斜长石包体;石英,呈他形粒状、浑圆状结构。角闪石呈半自形柱粒状结构,多色性明显,局部被黑云母交代;黑云母,呈片状,多色性明显(黄绿色、淡绿色、黄褐色等),部分褐铁矿化;基质由斜长石、钾长石、石英、角闪石、

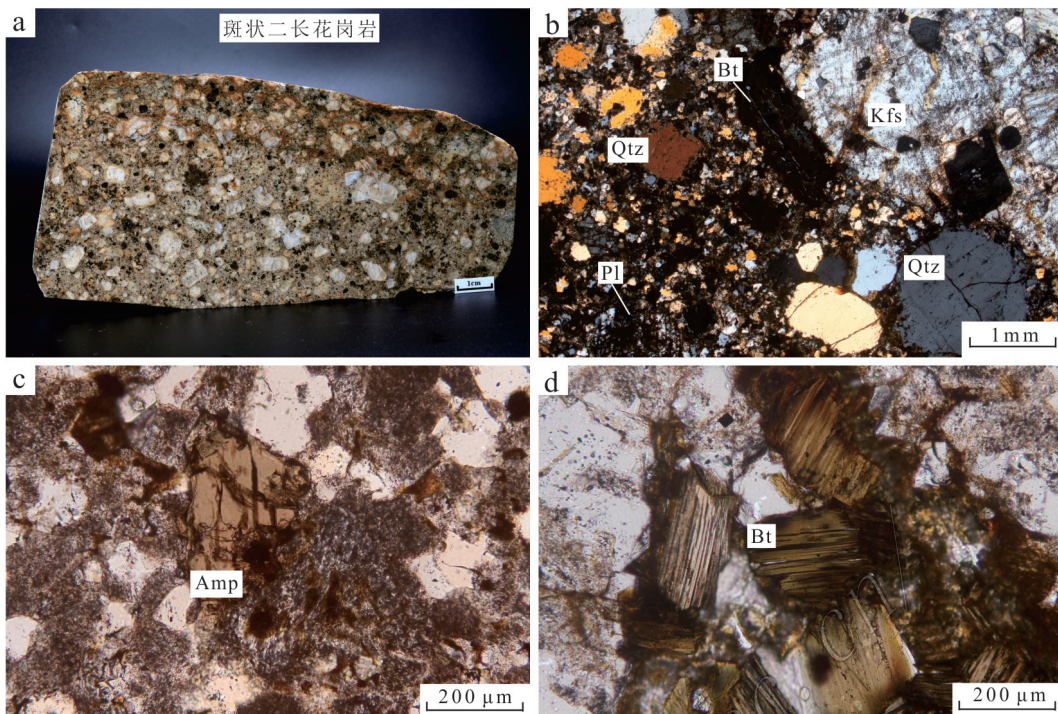


图4 毛登矿区斑状二长花岗岩相学照片

a. 斑状二长花岗岩手标本照片;b. 斑状二长花岗岩镜下照片(+);c. 镜下角闪石照片(-);d. 镜下黑云母照片(-)

Amp—角闪石; Bt—黑云母; Kfs—钾长石; Pl—斜长石; Qtz—石英

Fig. 4 Petrographic photos of representative porphyritic monzogranite in the Maodeng deposit

a. Hand specimen of porphyritic monzogranite; b. Microphotograph of porphyritic monzogranite(+); c. Microphotograph of amphibole(-);
d. Microphotograph of biotite(-)
Amp—Amphibole; Bt—Biotite; Kfs—K-feldspar; Pl—Plagioclase; Qtz—Quartz

黑云母等组成,粒径0.05~0.40 mm,杂乱分布。长石(斜长石+钾长石)(含量10%~35%),呈半自形-他形粒状结构,高岭土化明显;石英(含量10%~15%),呈他形粒状结构,杂乱分布;角闪石(少量),呈他形粒状结构,零散分布,多色性明显,局部被黑云母交代;黑云母(少量),呈片状,多色性明显。副矿物由少量锆石、磷灰石等组成,零星分布。

岩石样品磨制探针片后,镜下观察选取新鲜未蚀变且背散射电子图像(BSE)显示化学成分均一的角闪石和黑云母,开展电子探针(EPMA)原位主量元素成分分析。探针片喷碳、BSE照相和EMPA测试分析工作均在河北省区域地质矿产调查研究所实验室完成。角闪石和黑云母矿物学成分分析在JXA-8230 EMPA型电子探针分析仪完成,实验测试加速电压15 kV,束流20 nA,束斑直径5 μm。主量元素的检出限为0.01%,标样矿物(括号内)分别是K(钾长石),Ca(方解石),Ti(金红石),Na、Al、Si(硬玉),Mg、Ni(镁橄榄石),Cr、Fe(铬铁矿),Mn(蔷薇

辉石),F(黄玉),Cl(石盐),P(磷灰石)等。

岩石样品破碎后至合适粒度,经人工淘洗、分选后在双目镜下挑选出自形程度较好的锆石颗粒,用环氧树脂固定、制靶。锆石靶由北京中科矿研检测技术有限公司制备,直径25 mm,厚5 mm。经透射光、反射光和阴极发光照相,观察、选择合适的锆石单矿物测试点位。斑状二长花岗岩锆石样品的U-Pb定年和微量元素原位成分分析测试工作在中国地质科学院矿产资源研究所LA-MC-ICP-MS实验室同时完成,采用单点激光剥蚀等离子质谱(LA-ICP-MS)方式,激光剥蚀系统为RESOLUTION S-155型193 nm准分子激光。U-Pb定年数据分析前用锆石GJ-1调试仪器,U、Th含量以锆石M127(Nasdala et al., 2008)为外标进行校正,测试流程参考侯可军等(2009);锆石微量元素含量利用SRM610作为外标、Si作内标的方法进行定量计算(Liu et al., 2008)。分析数据的离线处理采用软件ICPMsDataCal 4.3(Liu et al., 2008;侯可军等,

2009)完成,运用Isoplot3.0程序(Ludwig, 2003)计算、绘制锆石年龄谐和图。

3 分析结果

3.1 锆石微量元素特征及U-Pb年龄

阴极发光(CL)图像可知MD19-11锆石呈自形粒状结构,长约70~360 μm,宽约50~160 μm,大部分锆石显示清晰的震荡环带结构,属于典型的岩浆作

用形成的锆石。选择环带结构清晰的代表性锆石颗粒进行原位LA-ICP-MS微量元素和U-Pb年龄测试分析,结果见表1和表2。

3.1.1 微量元素特征

毛登斑状二长花岗岩锆石稀土元素总量(Σ REE)变化范围较大,为 $(335.08\sim630.80)\times10^{-6}$,轻稀土元素(LREE)为 $(10.93\sim23.95)\times10^{-6}$,重稀土元素(HREE)为 $(323.43\sim606.85)\times10^{-6}$ 。研究发现,饱和熔体或流体中结晶形成的热液锆石也具有岩浆锆

表1 毛登矿床斑状二长花岗岩锆石微量元素含量

Table 1 Trace elements in zircon of the porphyritic monzogranite in the Maodeng deposit

组分	MD19-11									
	4	5	6	7	9	11	14	18	19	20
$w(B)/10^{-6}$										
La	0.51	0.01	0.03	0.05	0.01	0.08	0.01	0.01	0.01	0.52
Ce	10.32	7.41	17.13	6.18	9.08	17.20	16.27	8.69	12.95	12.04
Pr	0.25	0.08	0.06	0.09	0.11	0.10	0.06	0.06	0.04	0.21
Nd	2.29	1.41	1.75	1.16	1.13	1.65	1.40	0.67	1.22	2.17
Sm	4.56	3.18	4.94	3.18	3.24	4.39	3.66	2.15	2.68	3.70
Eu	0.21	0.05	0.05	0.27	0.19	0.04	0.06	0.08	0.07	0.24
Gd	21.90	19.46	24.53	15.59	17.06	22.98	20.22	12.71	18.19	16.07
Tb	6.97	6.12	8.04	4.78	5.40	7.50	6.09	4.14	6.14	5.11
Dy	73.30	70.05	90.34	51.38	58.37	82.18	69.63	45.00	70.62	57.28
Ho	25.41	24.24	32.71	18.32	20.91	29.06	24.95	16.75	25.55	19.87
Er	106.90	103.99	138.59	77.48	87.88	125.30	106.17	71.91	108.37	84.15
Tm	20.51	19.84	27.14	14.90	17.16	24.34	21.08	14.49	21.57	16.74
Yb	183.40	177.87	239.57	134.68	154.47	222.28	187.99	132.24	191.03	151.59
Lu	35.75	33.61	45.94	26.07	29.72	41.85	36.32	26.18	36.32	28.53
Y	725.12	695.02	916.95	522.49	597.18	824.30	700.89	475.17	717.96	569.81
Hf	8907	8970	9811	8262	8613	9282	9635	8937	10021	8777
Ti	3.99	6.00	4.27	10.90	7.31	3.59	4.93	4.12	2.59	9.05
Ta	0.83	1.15	1.89	0.45	0.71	1.63	1.42	0.79	1.80	0.78
Nb	1.68	2.73	4.49	1.02	1.40	3.60	2.99	1.62	4.19	1.67
U	143.28	178.57	433.48	93.11	119.06	357.85	285.33	125.29	331.67	152.37
δ Eu	0.07	0.02	0.01	0.12	0.08	0.01	0.02	0.04	0.03	0.09
δ Ce	7.09	63.46	101.39	21.97	67.11	47.03	166.48	84.52	156.26	8.96
Σ REE	492.28	467.33	630.80	354.13	404.72	578.96	493.92	335.08	494.76	398.22
LREE	18.14	12.14	23.95	10.93	13.76	23.46	21.46	11.66	16.98	18.87
HREE	474.14	455.18	606.85	343.20	390.97	555.50	472.46	323.43	477.78	379.35
$T_{Ti}/^{\circ}C$	709	746	715	805	765	700	728	712	672	786
Δ NNNO	-3.7	-1.8	-0.5	-0.7	0.0	-0.7	0.6	0.7	-0.8	-0.6
Δ FMQ	-3.1	-1.2	0.1	-0.2	0.5	-0.1	1.2	1.3	-0.2	0.0
$lg(f(O_2))$	-19.6	-16.8	-16.2	-14.4	-14.6	-16.8	-14.8	-15.1	-17.6	-14.6
Ce^{4+}/Ce^{3+}	15	19	35	17	28	38	43	50	46	20

注:比值单位为1; T_{Ti} 为锆石Ti温度计,据Ferry等(2007)方法计算;lg($f(O_2)$)、 Δ NNNO、 Δ FMQ和 Ce^{4+}/Ce^{3+} 据Geo-f(O_2)软件程序Li等(2019)计算获得。

表2 毛登岩体的LA-ICP-MS锆石U-Pb分析数据

Table 2 LA-ICP-MS zircon U-Pb data of the granite in the Maodeng deposit

点号	$w(B)/10^{-6}$			Th/U	同位素比值			年龄/Ma					谐和度	
	Th	U	$^{207}\text{Pb}/^{235}\text{U}$		1σ	$^{206}\text{Pb}/^{238}\text{U}$	1σ	$^{207}\text{Pb}/^{235}\text{U}$	1σ	$^{206}\text{Pb}/^{238}\text{U}$	1σ	$^{207}\text{Pb}/^{206}\text{Pb}$		
MD19-11(斑状二长花岗岩)														
1	106	225	0.47	0.1651	0.0096	0.0219	0.0002	155	8	140	2	467	97	90%
2	125	264	0.48	0.1509	0.0068	0.0220	0.0003	143	6	140	2	195	106	98%
5	75	179	0.42	0.1606	0.0096	0.0221	0.0003	151	8	141	2	332	131	93%
6	175	433	0.40	0.1461	0.0051	0.0220	0.0003	138	5	140	2	122	81	98%
7	46	93	0.50	0.1431	0.0169	0.0218	0.0004	136	15	139	3	87	256	97%
8	126	268	0.47	0.1502	0.0073	0.0221	0.0003	142	6	141	2	176	113	99%
9	61	119	0.51	0.1502	0.0145	0.0221	0.0004	142	13	141	3	256	220	99%
10	72	157	0.45	0.1548	0.0112	0.0219	0.0003	146	10	140	2	276	172	95%
11	155	358	0.43	0.1455	0.0055	0.0220	0.0003	138	5	140	2	106	87	98%
12	102	218	0.47	0.1598	0.0074	0.0220	0.0003	151	6	140	2	339	111	93%
13	154	327	0.47	0.1578	0.0086	0.0219	0.0003	149	8	140	2	306	128	93%
14	124	285	0.43	0.1503	0.0077	0.0219	0.0003	142	7	140	2	187	110	98%
15	78	155	0.50	0.1443	0.0116	0.0219	0.0003	137	10	139	2	167	172	98%
16	112	238	0.47	0.1333	0.0074	0.0219	0.0003	127	7	139	2	error	error	90%
18	53	125	0.42	0.1426	0.0138	0.0218	0.0003	135	12	139	2	100	209	97%
19	114	332	0.34	0.1449	0.0068	0.0219	0.0002	137	6	139	2	98	113	98%
20	75	152	0.49	0.1463	0.0097	0.0219	0.0003	139	9	140	2	122	143	99%

石的振荡环带特征(Elzbieta et al., 2004),因此,振荡环带不是岩浆锆石的专属特征。大量研究表明,岩浆锆石和热液锆石稀土元素组成特征不同,相对于后者,前者稀土元素总量较低,尤其是轻稀土元素含量明显偏小,稀土元素配分模式图更陡,更明显的Ce正异常(Sun et al., 1989)。毛登斑状二长花岗岩锆石亏损LREE,富集HREE,稀土元素配分模式图呈陡左倾,明显的Ce正异常($\delta\text{Ce}=7.09\sim166.48$)和Eu负异常($\delta\text{Eu}=0.01\sim0.12$)。稀土元素配分曲线落入岩浆锆石稀土元素配分曲线区域中(图5a),显示岩浆来源特征(Hoskin et al., 2000)。

3.1.2 U-Pb年龄

斑状二长花岗岩样品MD19-11中17颗(文中已剔除3颗谐和度低于90%的锆石数据)锆石LA-ICP-MS分析结果显示, $w(\text{Th})$ 为 $(46\sim175)\times10^{-6}$, $w(\text{U})$ 为 $(93\sim433)\times10^{-6}$, Th/U 比值 $0.39\sim0.5$,属岩浆成因锆石。在U-Pb谐和年龄图(图5b)中,投点均落在谐和线及其附近, $^{206}\text{Pb}/^{238}\text{U}$ 加权平均年龄为 $(140\pm0.9)\text{Ma}$ (MSWD=0.1; $n=17$)(表3),代表了斑状二长花岗岩形成年龄。

3.2 角闪石成分特征

角闪石是斑状二长花岗岩中主要的铁镁质矿

物,呈黄褐色,半自形柱状或粒状结构,解理明显(图4c),局部被黑云母交代蚀变。电子探针分析结果(表3)显示,角闪石主要成分 $w(\text{SiO}_2)$ 为44.1%~46.11%(平均45.3%), $w(\text{TiO}_2)$ 为0.81%~1.52%(平均1.21%), $w(\text{Al}_2\text{O}_3)$ 为5.13%~6.29%(平均5.77%), $w(\text{TFeO})$ 为22.38%~26.41%(平均24.36%), $w(\text{MnO}_2)$ 为0.27%~0.52%(平均0.38%), $w(\text{MgO})$ 为5.67%~8.09%(平均7.16%), $w(\text{CaO})$ 为9.57%~10.36%(平均10.02%), $w(\text{Na}_2\text{O})$ 为1.9%~2.22%(平均2.02%), $w(\text{K}_2\text{O})$ 为0.85%~1.17%(平均0.99%), $w(\text{F})$ 为1.39%~2.96%(平均2.46%), $w(\text{Cl})$ 为0.18%~0.53(平均0.27%),并还有少量的 Cr_2O_3 (<0.04%)和 NiO (<0.03%),表现出富铁、钙、氟和氯,贫镁、钠、钾的特征。

采用林文蔚等(1994)的计算方法获得角闪石 $\text{Fe}^{3+}/\text{Fe}^{2+}$ 值,并以23个氧原子为标准计算角闪石阳离子数及相关参数;角闪石 $\text{Ca}_B=1.57\sim1.72$, $\text{Na}_B=0.28\sim0.43$,根据国际矿物协会角闪石专业委员会报告,属于钙角闪石系列; $(\text{Na}+\text{K})_A=0.33\sim0.57$,在Leake(1997)提出的角闪石分类图解(图6a,b)中,样品投点分别落在铁角闪石和铁浅闪石范围。

3.3 黑云母成分特征

斑状二长花岗岩黑云母多呈浅黄褐色、粒

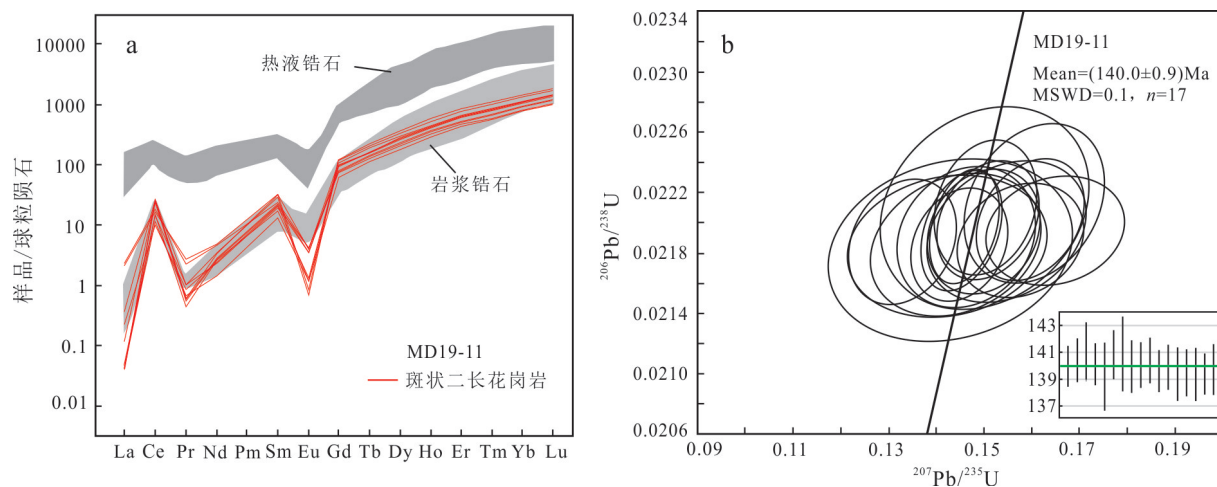


图5 毛登矿床斑状二长花岗岩锆石球粒陨石标准稀土元素配分图(a, 标准化值据Sun et al., 1989; 阴影区域数据参考自Hoskin, 2005)和锆石U-Pb谐和年龄图(b)

Fig. 5 Chondrite-normalized REE patterns (a, normalization values after Sun et al., 1989; the shading area data after Hoskin, 2005) and U-Pb concordia diagram (b) for the zircon of the porphyritic monzogranite in the Maodeng deposit

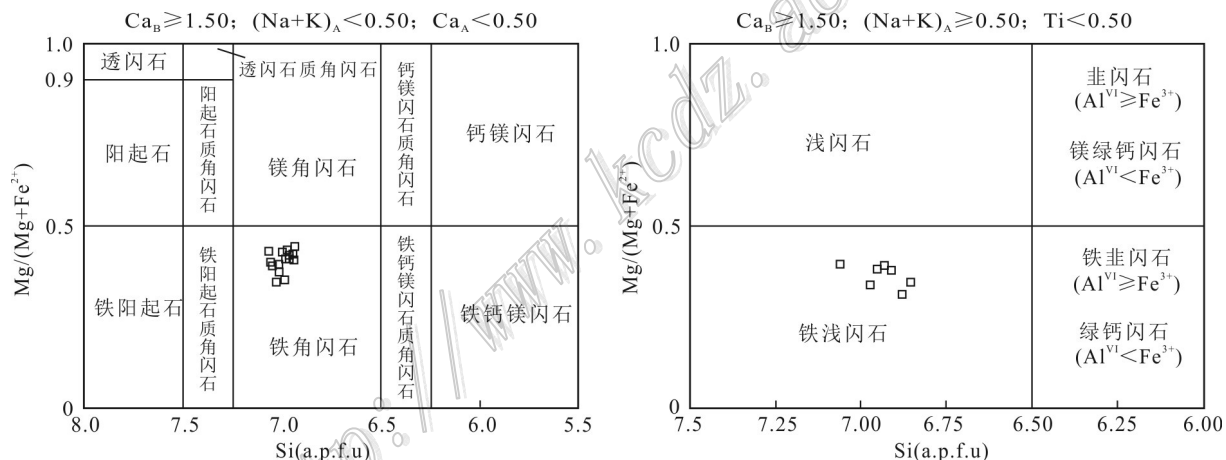


图6 毛登矿床斑状二长花岗岩角闪石分类图解(a, $(\text{Na}+\text{K})_A < 0.5$; b, $(\text{Na}+\text{K})_A \geq 0.5$, 据Leake et al., 1997)

Fig. 6 Classification of the amphibole (a, $(\text{Na}+\text{K})_A < 0.5$; b, $(\text{Na}+\text{K})_A \geq 0.5$, after Leake et al., 1997) of the porphyritic monzogranite in the Maodeng deposit

径0.2~0.6 mm,板片状结构,1组完全解理,整体较新鲜(图4d)。电子探针分析结果(表4)显示,黑云母的 $w(\text{SiO}_2)$ 为36.29%~37.56%(平均37.0%), $w(\text{TiO}_2)$ 为2.61%~4.06%(平均3.18%), $w(\text{Al}_2\text{O}_3)$ 为11.71%~12.47%(平均12.09%), $w(\text{TFeO})$ 为24.73%~28.53%(平均25.93%), $w(\text{K}_2\text{O})$ 为7.82%~9.16%(平均8.52%), $w(\text{MgO})$ 为6.21%~9.02%(平均8.06%), $w(\text{Na}_2\text{O})$ 为0.28%~0.49%(平均0.41%), $w(\text{F})$ 为0.92%~2.20%(平均1.46%), $w(\text{Cl})$ 为0.26%~0.63%(平均0.54%),还有少量的 $w(\text{MnO}_2)$ 为0.19%~0.27%(平均0.22%)、 w

(CaO) 为0.01%~0.11%(平均0.07%)和 $w(\text{Cr}_2\text{O}_3)$ 为0.05%~0.24%(平均0.14%)。总体来说,富Fe、F、Cl,贫Mg、Al;CaO含量均极低(贫Ca或无Ca),说明黑云母基本无绿泥石化或碳酸盐化(Kumar et al., 2010)。根据黑云母的化学成分,采用林文蔚等(1994)提出的富铝黑云母计算方法获得黑云母中 $\text{Fe}^{2+}/\text{Fe}^{3+}$ 值,并以22个氧原子为标准计算黑云母的阳离子数,结果见表4。

根据Foster(1960)提出的黑云母分类方法,在 $\text{Mg}-(\text{Al}^{\text{IV}}+\text{Fe}^{3+}+\text{Ti})-(\text{Fe}^{2+}+\text{Mn})$ 图解(图7a)中,斑状二

表3 毛登斑状二长花岗岩角闪石电子探针分析结果

Table 3 Electron microprobe analyses of amphibole from the porphyritic monzogranite in the Maodeng deposit

组分	MD19-11					MD19-73						
	1	3	6	8	9	1	2	3	4	5	6	
<i>w(B)/%</i>												
K ₂ O	1.00	0.88	0.90	1.15	1.17	0.99	1.01	1.02	1.03	0.87	0.92	
CaO	9.76	9.47	10.06	10.21	10.36	10.00	9.98	9.96	10.06	9.89	9.90	
TiO ₂	1.15	0.84	1.18	1.27	1.44	1.10	1.30	1.52	1.32	1.12	1.32	
Na ₂ O	1.91	1.95	1.91	2.00	2.00	1.95	2.00	2.06	2.18	1.99	2.01	
MgO	7.25	6.43	7.58	6.21	6.38	7.22	6.46	8.09	7.21	7.92	7.35	
Al ₂ O ₃	5.59	5.13	5.56	6.05	5.92	5.53	5.48	6.29	6.03	5.36	5.25	
氧化物 含量	SiO ₂	45.62	45.29	44.97	44.10	44.96	45.53	45.42	45.28	44.22	46.11	45.96
	Cr ₂ O ₃	0.00	0.00	0.03	0.02	0.02	0.00	0.01	0.01	0.02	0.03	0.02
	MnO	0.44	0.52	0.35	0.51	0.38	0.38	0.41	0.27	0.32	0.30	0.35
	TFeO	24.69	26.21	23.88	25.99	25.09	24.42	25.18	22.38	23.44	23.23	24.17
	NiO	0	0.02	0.01	0.02	0.01	0	0	0.02	0	0	0
	F	1.39	2.46	2.32	2.81	1.98	2.51	2.13	2.29	2.48	2.53	2.45
	Cl	0.34	0.29	0.21	0.53	0.33	0.29	0.29	0.18	0.28	0.19	0.22
	总和	99.14	99.49	98.96	100.87	100.04	99.92	99.67	99.37	98.59	99.54	99.92
基于23个氧原子计算的阳离子数												
T	Si	6.98	7.02	6.96	6.86	6.97	7.01	7.04	6.94	6.93	7.07	7.06
	Al ^{IV}	1.01	0.94	1.01	1.11	1.03	0.99	0.96	1.06	1.07	0.93	0.94
	Ti	0.01	0.05	0.03	0.04	0	0	0	0	0	0	0
C	Al ^{VI}	0	0	0	0	0.05	0.02	0.04	0.07	0.04	0.04	0.01
	Ti	0.13	0.05	0.11	0.11	0.17	0.13	0.15	0.18	0.16	0.13	0.15
	Cr	0	0	0	0	0	0	0	0	0	0	0
	Fe ³⁺	0.79	0.93	0.70	0.65	0.36	0.64	0.51	0.56	0.46	0.62	0.58
	Mg	1.66	1.49	1.75	1.44	1.48	1.66	1.49	1.85	1.68	1.81	1.68
	Fe ²⁺	2.37	2.46	2.39	2.73	2.89	2.51	2.76	2.31	2.61	2.36	2.52
	Mn	0.06	0.07	0.05	0.07	0.05	0.05	0.05	0.04	0.04	0.04	0.05
B	Fe ²⁺	0	0	0	0	0	0	0	0	0	0	0
	Ca	1.60	1.57	1.67	1.70	1.72	1.65	1.66	1.63	1.69	1.62	1.63
	Na	0.40	0.43	0.33	0.30	0.28	0.35	0.34	0.37	0.31	0.38	0.37
A	Na	0.17	0.16	0.24	0.30	0.32	0.23	0.26	0.25	0.35	0.22	0.23
	K	0.20	0.17	0.18	0.23	0.23	0.19	0.20	0.20	0.21	0.17	0.18
相关参数	Si*	8.73	8.79	8.61	8.51	8.62	8.73	8.76	8.54	8.55	8.76	8.78
	Al ^{II}	1.01	0.94	1.01	1.11	1.08	1.00	1.00	1.14	1.11	0.97	0.95
	Mg*	2.24	2.23	2.29	1.99	1.90	2.19	1.99	2.24	2.09	2.32	2.17
	Al*	-1.59	-1.50	-1.57	-1.59	-1.62	-1.60	-1.58	-1.60	-1.63	-1.59	-1.62
	T/°C	718	709	737	753	735	719	714	747	746	714	711
	P/MPa	179	145	182	227	214	177	175	239	229	160	151
	深度/km	6.8	5.5	6.9	8.6	8.1	6.7	6.6	9.0	8.6	6.1	5.7
	ΔNNO	-0.3	-0.3	-0.2	-0.7	-0.9	-0.4	-0.7	-0.3	-0.6	-0.2	-0.4
	lg/(O ₂)	-16.1	-16.3	-15.5	-15.6	-16.2	-16.1	-16.6	-15.4	-15.6	-16.1	-16.4
	H ₂ O _{melt} /%	4.0	4.4	4.1	4.0	3.9	3.9	4.0	3.9	3.8	4.0	3.8
	(Na+K) _A	0.36	0.33	0.42	0.53	0.56	0.43	0.46	0.45	0.56	0.39	0.41

续表 3

Continued Table 3

组分	MD19-73					MD19-75					
	7	8	9	10	2	3	5	6	9	10	11
<i>w(B)/%</i>											
K ₂ O	0.88	1.04	1.01	1.06	1.11	0.91	0.85	0.99	1.02	1.00	0.97
CaO	9.90	10.02	10.13	10.26	9.99	10.23	10.02	10.12	10.12	10.12	9.90
TiO ₂	1.27	1.23	1.18	1.26	1.36	1.26	1.18	1.10	0.81	1.52	0.93
Na ₂ O	2.07	2.10	1.97	2.22	2.19	1.97	1.90	2.13	2.16	2.00	2.17
MgO	7.86	6.91	7.75	7.15	5.67	7.56	7.70	7.33	7.47	7.51	6.46
Al ₂ O ₃	5.69	6.18	6.13	6.01	6.21	5.96	5.78	5.77	5.40	6.15	5.59
氧化物	SiO ₂	45.76	44.67	45.39	45.09	44.17	45.71	45.77	45.91	45.98	45.34
含量	Cr ₂ O ₃	0.01	0	0	0	0.04	0	0.03	0	0	0.01
MnO	0.31	0.38	0.31	0.37	0.48	0.38	0.37	0.38	0.42	0.36	0.48
TFeO	23.75	24.42	23.50	24.14	26.41	23.92	23.61	23.77	24.20	23.48	25.95
NiO	0	0	0.02	0.03	0	0	0.01	0.01	0	0	0
F	2.70	2.58	2.10	2.59	2.34	2.95	2.42	2.66	2.96	2.65	2.80
C1	0.21	0.29	0.21	0.24	0.34	0.20	0.20	0.21	0.32	0.22	0.39
总和	100.41	99.82	99.7	100.42	100.31	101.05	99.84	100.38	100.86	100.37	100.96
基于23个氧原子计算的阳离子数											
Si	6.98	6.92	6.94	6.96	6.88	6.97	7.00	7.05	7.06	6.94	6.98
T	Al ^{IV}	1.02	1.08	1.06	1.04	1.12	1.03	1.00	0.95	0.94	1.06
	Ti	0	0	0	0	0	0	0	0	0	0
	Al ^{VI}	0	0.05	0.05	0.05	0.02	0.04	0.04	0.09	0.04	0.06
	Ti	0.14	0.14	0.14	0.15	0.16	0.14	0.14	0.13	0.09	0.18
	Cr	0	0	0	0	0.01	0	0	0	0	0
C	Fe ³⁺	0.71	0.58	0.63	0.44	0.57	0.60	0.68	0.45	0.54	0.54
	Mg	1.79	1.60	1.77	1.64	1.32	1.72	1.76	1.68	1.71	1.71
	Fe ²⁺	2.31	2.58	2.38	2.67	2.87	2.45	2.34	2.61	2.56	2.47
	Mn	0.04	0.05	0.04	0.05	0.06	0.05	0.05	0.05	0.05	0.06
B	Fe ²⁺	0	0	0	0	0	0	0	0	0	0
	Ca	1.62	1.66	1.66	1.70	1.67	1.67	1.64	1.66	1.66	1.63
	Na	0.38	0.34	0.34	0.30	0.33	0.33	0.36	0.34	0.34	0.37
A	Na	0.23	0.29	0.25	0.36	0.33	0.25	0.20	0.30	0.31	0.25
	K	0.17	0.21	0.20	0.21	0.22	0.18	0.16	0.19	0.20	0.19
	Si*	8.67	8.59	8.59	8.58	8.60	8.63	8.69	8.69	8.74	8.58
	Al ^T	1.02	1.13	1.10	1.09	1.14	1.07	1.04	1.04	0.98	1.11
	Mg*	2.29	2.07	2.25	2.06	1.81	2.19	2.27	2.14	2.23	2.13
	Al*	-1.60	-1.57	-1.57	-1.63	-1.57	-1.53	-1.50	-1.57	-1.66	-1.56
	T/°C	727	740	739	741	738	734	725	724	717	741
相关参数	P/MPa	186	236	225	219	241	209	195	196	164	228
	深度/km	7.0	8.9	8.5	8.3	9.1	7.9	7.4	7.4	6.2	8.6
	ΔNNO	-0.3	-0.6	-0.3	-0.6	-1.0	-0.4	-0.3	-0.5	-0.3	-0.6
	lgf(O ₂)	-15.8	-15.8	-15.5	-15.8	-16.3	-15.8	-15.9	-16.1	-16.1	-15.7
	H ₂ O _{melt} /%	3.9	4.1	4.1	3.8	4.1	4.3	4.4	4.1	3.6	4.0
	(Na+K) _A	0.40	0.50	0.44	0.57	0.55	0.43	0.37	0.49	0.51	0.45

注:比值单位为1;T、ΔNNO、lgf(O₂)、H₂O_{melt}据Ridolfi等(2008;2010)计算获得;P据Schmidt(1992)计算获得;Si*、Mg*、Al*为计算温度、氧逸度、压力公式中的过程变量。

表4 毛登矿床斑状二长花岗岩黑云母电子探针分析结果

Table 4 Electron microprobe analyses of biotite from the porphyritic monzogranite in the Maodeng deposit

组分及对比项目	MD19-73					MD19-75				
	1	2	3	4	5	1	3	4	5	6
<i>w(B)/%</i>										
SiO ₂	36.52	37.09	37.25	37.56	37.25	37.16	36.29	37.38	36.59	36.90
TiO ₂	3.46	4.06	3.25	2.68	3.28	2.61	3.38	2.92	3.35	2.78
Al ₂ O ₃	12.05	12.03	11.71	12.47	12.23	11.84	12.36	11.92	12.32	11.98
TFeO	26.51	26.82	25.31	26.67	25.29	24.73	28.53	24.98	25.06	25.36
MnO	0.21	0.22	0.19	0.20	0.20	0.24	0.24	0.24	0.27	0.23
MgO	7.75	7.43	8.05	8.59	8.10	8.92	6.21	9.02	8.21	8.32
CaO	0.09	0.06	0.11	0.07	0.11	0.04	0.09	0.01	0.07	0.09
Na ₂ O	0.49	0.28	0.46	0.48	0.43	0.46	0.32	0.39	0.41	0.41
K ₂ O	8.19	8.83	8.75	7.82	8.27	8.97	8.07	9.16	8.67	8.51
Cr ₂ O ₃	0.05	0.09	0.11	0.12	0.13	0.16	0.17	0.19	0.20	0.24
F	0.92	0.95	1.33	1.27	1.64	1.98	0.96	2.20	1.96	1.41
Cl	0.63	0.60	0.43	0.26	0.59	0.57	0.61	0.52	0.62	0.59
总和	96.87	98.46	96.95	98.19	97.52	97.68	97.23	98.93	97.73	96.82
以22个氧原子为基准计算的阳离子数及参数										
Si	5.77	5.77	5.87	5.81	5.84	5.85	5.76	5.82	5.76	5.83
Al ^{IV}	2.23	2.21	2.13	2.19	2.16	2.15	2.24	2.18	2.24	2.17
Al ^{VI}	0.01	0	0.04	0.09	0.10	0.05	0.07	0.01	0.05	0.07
Al ^T	2.24	2.21	2.17	2.28	2.26	2.20	2.31	2.19	2.29	2.23
Ti	0.41	0.48	0.38	0.31	0.39	0.31	0.40	0.34	0.40	0.33
Fe ³⁺	0.40	0.44	0.40	0.43	0.47	0.29	0.46	0.30	0.38	0.37
Fe ²⁺	3.10	3.06	2.94	3.03	2.85	2.97	3.33	2.96	2.93	2.99
Mn	0.03	0.03	0.03	0.03	0.03	0.03	0.03	0.03	0.04	0.03
Mg	1.82	1.72	1.89	1.98	1.89	2.09	1.47	2.10	1.93	1.96
Ca	0.02	0.01	0.02	0.01	0.02	0.01	0.01	0	0.01	0.02
Na	0.15	0.08	0.14	0.14	0.13	0.14	0.10	0.12	0.12	0.12
K	1.65	1.75	1.76	1.54	1.65	1.80	1.64	1.82	1.74	1.72
Mg/(Fe+Mg)	0.34	0.33	0.36	0.36	0.36	0.39	0.28	0.39	0.37	0.37
Fe/(Fe+Mg)	0.66	0.67	0.64	0.64	0.64	0.61	0.72	0.61	0.63	0.63
Fe ²⁺ /(Fe ²⁺ +Mg)	0.63	0.64	0.61	0.60	0.60	0.59	0.69	0.59	0.60	0.60
TFeO/(TFeO+MgO)	0.77	0.78	0.76	0.76	0.76	0.74	0.82	0.73	0.75	0.75
<i>t/°C</i>	692	712	683	650	685	652	684	669	689	660
lg(fO ₂)	-17.1	-16.5	-17.3	-18.3	-17.3	-18.3	-17.3	-17.8	-17.2	-18.0

注:比值单位为1; *t*据Henry等(2002)、Henry等(2005)计算获得; lg(fO₂)据Wones等(1965)计算获得。

长花岗岩黑云母大多数落在铁质黑云母区域,显示了富Fe的矿物化学特征,是壳源型花岗岩特有的标型矿物(叶茂等,2017)。黑云母的成因类型分为岩浆型和热液型,前者形成于岩浆结晶过程,后者形成于热液蚀变过程。岩相学特征显示,斑状二长花岗岩黑云母多呈自形-半自形片状结构,有锯齿状特征,多色性明显,呈黄褐色、褐色(图4d),表现出岩浆黑云母特征(唐攀等,2017)。 $Fe^{2+}/(Fe^{2+}+Mg)$ 值是岩浆氧化态的重要标志,斑状二长花岗岩黑云母 $Fe^{2+}/(Fe^{2+}+Mg)$ 值为0.56~0.69(平均值为0.60),变化范围均较小,显示测试黑云母未遭受后期流体作用改造

(Stone, 2000),指示了其岩浆成因。在黑云母10TiO₂-TFeO-MgO图解(图7b)中,投点多数落在岩浆黑云母范围内,少数位于岩浆黑云母与重结晶黑云母过渡区,暗示原生岩浆黑云母受后期轻度的次生改造作用(如重结晶作用)。

4 讨 论

4.1 成岩时代

前人对大兴安岭南段成矿带多个典型矿床开展了成岩年代学研究,认为燕山晚期花岗质岩浆侵位

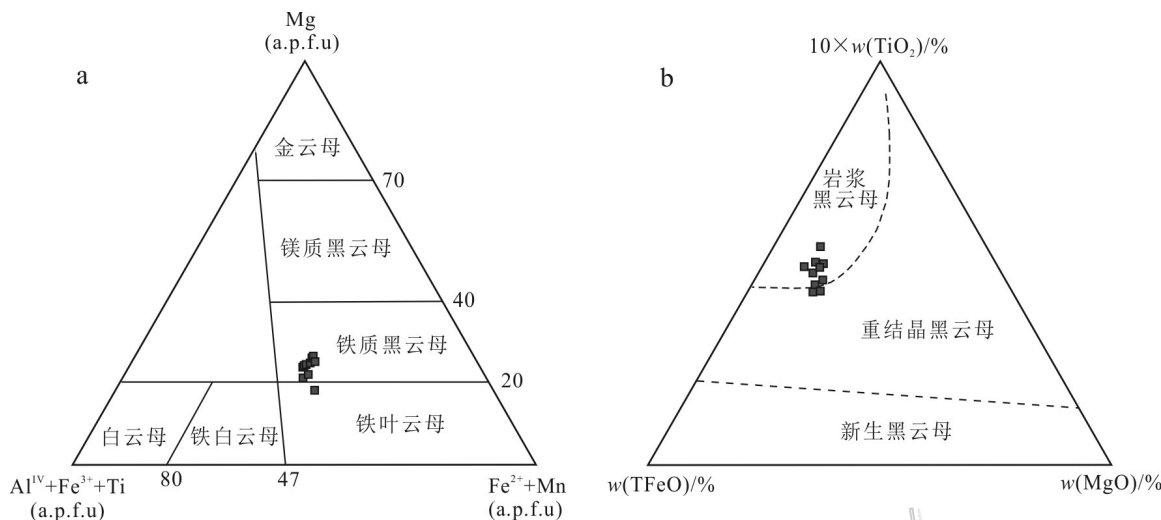


图7 毛登矿区斑状二长花岗岩黑云母分类图解(a, 据 Foster, 1960)和 $10\text{TiO}_2\text{-TFeO-MgO}$ 图解(b, 据 Nchit et al., 2005)
Fig. 7 Classification (a, after Foster, 1960) and $10\text{TiO}_2\text{-TFeO-MgO}$ diagram of the biotite from the porphyritic monzogranite in the Maodeng deposit (b, after Nchit et al., 2005)

与区内 Sn、Pb、Zn、Mo、Cu、Ag、Fe 等金属成矿作用关系密切(毛景文等, 2005; 2013; 周振华等, 2010; 翟德高等, 2012)。王长明等(2006)研究大兴安岭南段金属矿成矿时空结构表明, 区内锡成矿作用主要集中在燕山晚期; 季根源等(待刊)研究认为, 大兴安岭南段主要锡多金属矿床与成矿关系密切的花岗质岩体侵入时代为 129~149 Ma, 成岩时代峰值 137~140 Ma。

本次利用 LA-ICP-MS 锆石 U-Pb 法获得毛登矿区斑状二长花岗岩锆石结晶年龄为 $(140 \pm 0.9)\text{ Ma}$, 代表了斑状二长花岗岩侵位年龄, 与矿区内的 LA-ICP-MS 锆石 U-Pb 等时线年龄($(139 \pm 3.2)\text{ Ma}$, 季根源等, 待刊), 以及辉钼矿 Re-Os 同位素等时线年龄($(139 \pm 3.9)\text{ Ma}$, 笔者未发表数据)在误差范围内基本一致, 均发生在早白垩世。毛登矿区成岩(矿)年龄与周边典型锡、钼多金属矿床的成岩(矿)年龄相似, 如维拉斯托 Sn-Cu-Pb-Zn-Ag 多金属矿床锆石 U-Pb 年龄 136 Ma, 辉钼矿 Re-Os 年龄 136.8~138.8 Ma, 碱长花岗岩锆石 U-Pb 年龄 137~138 Ma(刘瑞麟等, 2018); 查木罕 W-Mo-Sn 矿床辉钼矿 Re-Os 年龄为 140 Ma, 二长花岗岩独居石 U-Pb 年龄为 137~139 Ma(Zhang et al., 2019); 白音查干 Sn-Ag 多金属矿床电气石花岗斑岩锆石 U-Pb 年龄 140.5 Ma, 花岗斑岩锆石 U-Pb 年龄 143.4 Ma, 锡石 U-Pb 年龄 140 Ma(李睿华, 2019); 敖伦花 Mo-Cu 矿床二长花岗斑岩锆石 U-Pb 年龄 134 Ma, 辉钼矿 Re-Os 年龄 132.1 Ma(马星华

等, 2009); 小东沟 Mo 矿床斑状花岗岩锆石 U-Pb 年龄 134 Ma, 辉钼矿 Re-Os 年龄 138 Ma(覃峰等, 2008; 2009); 半砬山 Mo 矿床花岗斑岩锆石 U-Pb 年龄 133.5 Ma, 辉钼矿 Re-Os 年龄 136.1 Ma(Zhang et al., 2010; Shu et al., 2016)。上述这些都反映出, 大兴安岭南段西坡锡林浩特-锡林郭勒 Sn-Ag-Cu-Pb-Zn-Mo 成矿亚带包括毛登在内的多数锡、钼多金属矿床为大兴安岭南段燕山晚期岩浆活动的产物。

4.2 成岩物理化学条件

花岗质岩浆的来源及其演化时的温度、压力、氧逸度等原始信息制约着成矿元素在熔体相-矿物相-流体相之间的迁移和富集(Stempok, 1990; Kepper et al., 1991; 林文蔚等, 1994), 而利用岩浆岩中矿物元素成分特征, 可以推演矿物结晶形成时岩浆的物理化学特征(包括温度、压力和氧逸度等)(Speer, 1984; 赵振华, 2010; Temizel et al., 2014)。

4.2.1 温度与压力

锆石微量元素组成特征可为母岩浆的性质和演化过程提供重要的地球化学信息(钟玉芳等, 2000), 利用锆石中 Ti 含量可估算形成时岩浆温度, 广泛应用于岩浆岩、变质岩和沉积岩的岩石结晶温度计算(Hoskin et al., 2000; Belousova et al., 2006; Ferry et al., 2007)。本文运用 LA-ICP-MS 测得锆石 $w(\text{Ti})$ 为 $(3.99 \pm 10.9) \times 10^{-6}$ (平均 5.67×10^{-6}), 利用 Ferry 等(2007)提出的锆石 Ti 温度计, 计算获得锆石结晶温度 672~805°C(平均 734°C)。Ridolfi 等(2010)利用

前人的岩石学实验数据进行经验标定,根据角闪石化学成分拟合出角闪石温压计,并得到广泛的认可和应用(段登飞等,2017;龚林等,2018;程贤达等,2019)。本文采用 Ridolfi 等(2010)提出的角闪石结晶温度计算公式:

$$t = -151.487 \text{Si}^* + 3041,$$

$$\text{Si}^* = \text{Si} + \text{Al}^{IV}/15 - 2\text{Ti}^{IV} - \text{Al}^{VI}/2 + \text{Ti}^{VI}/1.8 + \text{Fe}^{3+}/9 + \text{Fe}^{2+}/3.3 + \text{Mg}/26 + \text{Ca}_B/5 + \text{Na}_B/1.3 - \text{Na}_A/15 + \text{K}_A/2.3$$

计算获得角闪石结晶时的温度为 709~753°C(平均 729°C)。前人研究表明,在高温高压环境下,黑云母中 Ti 含量受温度的影响明显,并根据铝质变泥质岩熔融产物中黑云母 Ti 含量与其结晶温度的相关性提出经验的黑云母 Ti 饱和温度计算公式(Henry et al., 2002; 2005)。Sarjoughian 等(2015)研究发现,该黑云母 Ti 饱和温度计算公式也可适用于花岗质岩浆岩。本文对毛登矿区斑状二长花岗中黑云母斑晶开展了电子探针分析,利用黑云母 Ti 饱和温度计,计算获得黑云母结晶时温度为 650~712°C(平均 678°C)。由 Bowen 反应序列可知,随着岩浆的冷却,角闪石先于黑云母结晶,造成角闪石结晶温度高于黑云母结晶温度,与上述计算结果一致。

已有的研究指出,对于花岗岩成岩压力的计算:花岗岩中若存在角闪石+黑云母矿物组合,角闪石结晶完好时,角闪石全铝压力计的计算结果比较可靠;角闪石结晶不够完好,而黑云母矿物结晶完好时,则选择黑云母全铝压力计;若花岗岩不存在角闪石,利用黑云母全铝压力计获得的压力结果可能有较大的误差,黑云母不适合作为全铝压力计(康志强等,1994)。斑状二长花岗岩角闪石、黑云母矿物结晶较好,符合运用角闪石全铝压力计计算成岩压力的前提条件。Schmidt(1992)提出的角闪石全铝压力计: $P(\text{MPa}) = (4.76\text{Al}^T - 3.01) \times 10^8$ 适用于大多数钙碱性岩体的结晶压力估算(汪洋,2014),应用较为广泛(刘春花等,2013; 刘学龙等,2013; 向坤等,2019; 刘梓等,2020)。本文利用角闪石全铝压力计(Schmidt, 1992)获得角闪石结晶时压力 145~241 MPa(平均 198 MPa)。形成深度采用公式 $P = \rho g D$ 计算, $\rho = 2700 \text{ kg/m}^3$, $g = 9.8 \text{ m/s}^2$, 得出角闪石形成深度为 5.5~9.1 km(平均 7.5 km)。角闪石全铝压力计所获得的结晶压力接近固相线压力,所以角闪石压力计对应的成岩深度为斑状二长花岗岩体的侵位深度。

4.2.2 氧逸度与含水量

岩浆演化时的氧逸度是金属成矿重要的先决条

件之一,对成矿元素的迁移、富集起着非常重要的作用(张聚全等,2018)。目前,矿物氧逸度计常用来计算岩浆演化时的氧逸度,随着 EMPA、LA-ICP-MS 等矿物原位微区分析技术的发展,基于角闪石、黑云母以及锆石主、微量元素计算岩浆氧逸度的应用越来越广泛。岩浆含水量同样对岩浆演化和金属成矿有着重要的影响(Richards, 2003)。

由 Ferry 等(2007)提出的锆石 Ti 温度计算公式和 Trail 等(2012)提出的岩浆熔体氧逸度经验公式应用较广,但锆石的 La、Pr 含量低于检测线往往导致计算的氧逸度范围较大(罗雕等,2020)。本文利用 Li 等(2019)编写的 Geo-f(O₂) 软件程序,计算获得锆石结晶时岩浆氧逸度 $\lg f(O_2)$ 为 -19.6~-14.4(平均 -16.0), 相对氧逸度 $\Delta NNO - 3.7 \sim \Delta NNO + 0.7$ (平均 $\Delta NNO - 0.7$), $\Delta FMQ - 3.1 \sim \Delta FMQ + 1.3$ (平均 $\Delta FMQ - 0.2$), 氧逸度区间跨度较大,处于较低的氧逸度环境。

Spear(1981)和 Anderson 等(1995)研究认为,岩浆氧逸度的变化影响角闪石 Fe²⁺/Fe³⁺值,低氧逸度时较高的 Fe²⁺/Fe³⁺值有助于 Al 进入角闪石晶格,相反的,高氧逸度时 Fe²⁺/Fe³⁺值降低,角闪石中 Al 含量降低。本文根据 Ridolfi 等(2008; 2010)提出的利用角闪石矿物元素组成计算其结晶时寄主岩浆的氧逸度以及含水量,结果显示角闪石结晶时具相同的物理化学条件,熔体的相对氧逸度 $\Delta NNO - 1.0 \sim \Delta NNO - 0.2$ (平均 $\Delta NNO - 0.5$), 氧逸度 $\lg f(O_2)$ 为 -16.6~-15.4(平均 -16.0), 显示较低的氧逸度环境;岩浆含水量 H₂O_{melt} 为 3.6%~4.4%(平均 4.0%),显示较高的含水量,对岩浆活动期后的矿化作用是有利的。

研究认为,黑云母的 Fe 和 Mg 含量与形成时岩浆氧逸度关系密切,与磁铁矿和钾长石共生的黑云母可以通过 Fe²⁺、Fe³⁺ 和 Mg²⁺ 的原子百分数来估算黑云母形成时的氧逸度(Wones et al., 1965; Henry et al., 2005)。斑状二长花岗岩显微镜下发现黑云母、钾长石与磁铁矿共生矿物组合,因此,符合估算氧逸度的先决条件。在黑云母 Fe³⁺-Fe²⁺-Mg²⁺ 图解(图 8a)中,样品投点落在 Ni-NiO 缓冲线附近,反映出黑云母结晶时寄主岩浆氧逸度较低。另外,根据 Wones 等(1965)的 $P(\text{H}_2\text{O}) = 207.0 \text{ MPa}$ 条件下,黑云母的 $\lg f(O_2) - t$ 图解(图 8b),根据黑云母 Ti 饱和温度计获得的黑云母结晶时温度,利用 $\lg f(O_2) = 10.9 - 27000/T(\text{K})$ (Wones et al., 1965) 估算与黑云母平衡的岩浆氧逸度为 -18.3~-16.5(平均 -17.5),显示较低的氧逸度环境。

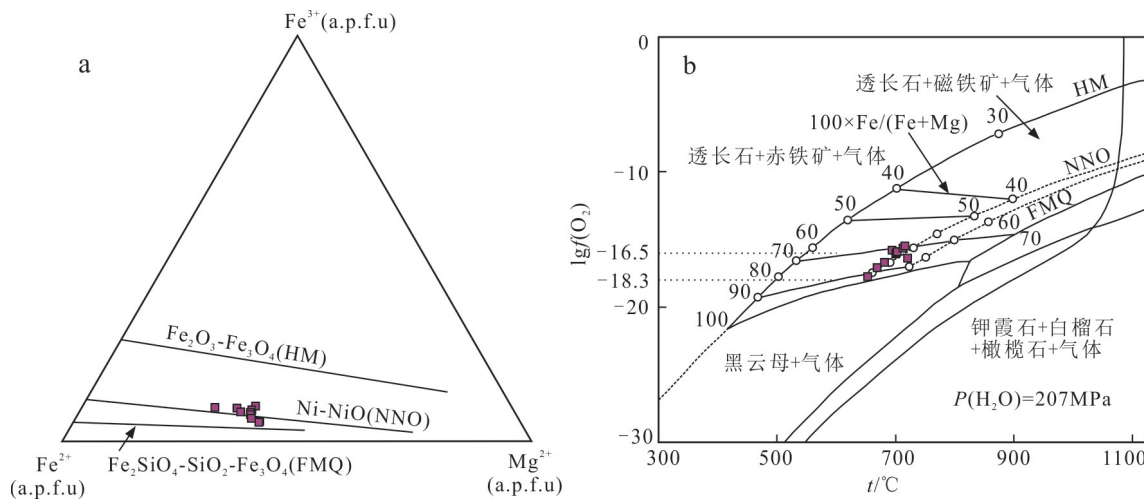


图8 毛登矿区斑状二长花岗岩黑云母 Fe^{3+} - Fe^{2+} - Mg^{2+} 图解(a, 据Wones et al., 1965)和 $\lg(f(\text{O}_2))$ - t 图解(b, 据Wones et al., 1965)

Fig. 8 Diagrams of Fe^{3+} - Fe^{2+} - Mg^{2+} (a, after Wones et al., 1965) and $\lg(f(\text{O}_2))$ - t (b, after Wones et al., 1965) of the biotite from the porphyritic monzogranite in the Maodeng deposit

综上可知,毛登斑状二长花岗岩浆演化过程中先晶出锆石、角闪石,后晶出黑云母,三者晶出时寄主岩浆温度分别为734°C、729°C和678°C,氧逸度分别为-16.0、-16.0、-17.5,表明随着岩浆的演化,温度逐渐降低,岩浆氧逸度逐渐减小(图9)。

4.3 岩石成因

花岗岩中角闪石和黑云母矿物元素成分,尤其是 $\text{Mg}/(\text{Fe}+\text{Mn})$ 等含量可以指示岩石类型,反演岩浆源区

的性质和构造环境(向坤等,2019;张忠坤等,2020)。

4.3.1 成因类型

前人对大兴安岭南段广泛发育的燕山晚期成矿花岗岩类型还未达成一致观点,多数认为属于A型花岗岩,包括巴尔哲、边家大院、黄岗等(邵济安等,2010;周振华等,2010;杨武斌等,2011;王喜龙等,2014),少数认为属于I型花岗岩,包括维拉斯托、白音查干等(Wang et al., 2017;张天福等,2018;李睿华,2019)。

黑云母的主量元素组成特征可以指示花岗岩成因类型和源区特征(Wones et al., 1965; Abdel-Rahman, 1994; Bi et al., 2009)。Abdel-Rahman(1994)统计全球大量不同构造环境岩体中黑云母元素成分,认为A型花岗岩黑云母相对富铁,I型和S型分别富镁和富铝,并根据统计结果提出了黑云母元素成分构造判别图解(图9a),可用来区分非造山碱性岩系(A型花岗岩,A区)、造山钙碱系(I型花岗岩,C区)和过铝系(S型,P区)的岩体,并指出A区岩系的黑云母富铁,近铁云母,C区岩系的富镁,P区岩系的富铝。Shabani等(2003)研究了加拿大阿巴拉契地区古生代不同成因花岗岩黑云母的矿物化学特征,认为黑云母主量元素组成特征能够指示母岩浆原始特征。本次研究的阿鲁包格山斑状二长花岗岩中黑云母在 $\text{Mg}-(\text{Al}^{\text{IV}}+\text{Fe}^{3+}+\text{Ti})-(\text{Fe}^{2+}+\text{Mn})$ 图解(图7a)中,投点均落在铁质黑云母区域,在黑云母 $\text{MgO}-\text{TFeO}-\text{Al}_2\text{O}_3$ 成因环境判别图解(图10a)中,投点均落在非造山的碱性岩套区域,在黑云母 $\text{Fe}/(\text{Fe}+\text{Mg})-\Sigma\text{Al}$ 图解(图10b)中,投点均落入A型花岗岩区域。因此认为,毛登矿

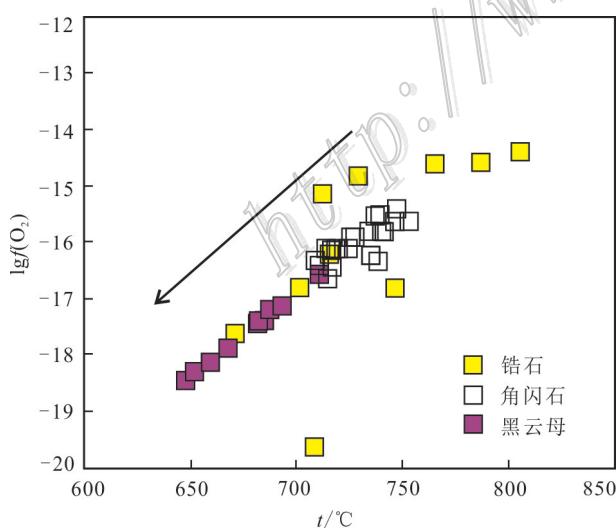


图9 毛登矿区斑状二长花岗岩岩体 $\lg(f(\text{O}_2))$ 与锆石、角闪石和黑云母的结晶温度(t)图解

Fig. 9 $\lg(f(\text{O}_2))$ versus t of zircon, amphibole and biotite from the porphyritic monzogranite in the Maodeng deposit

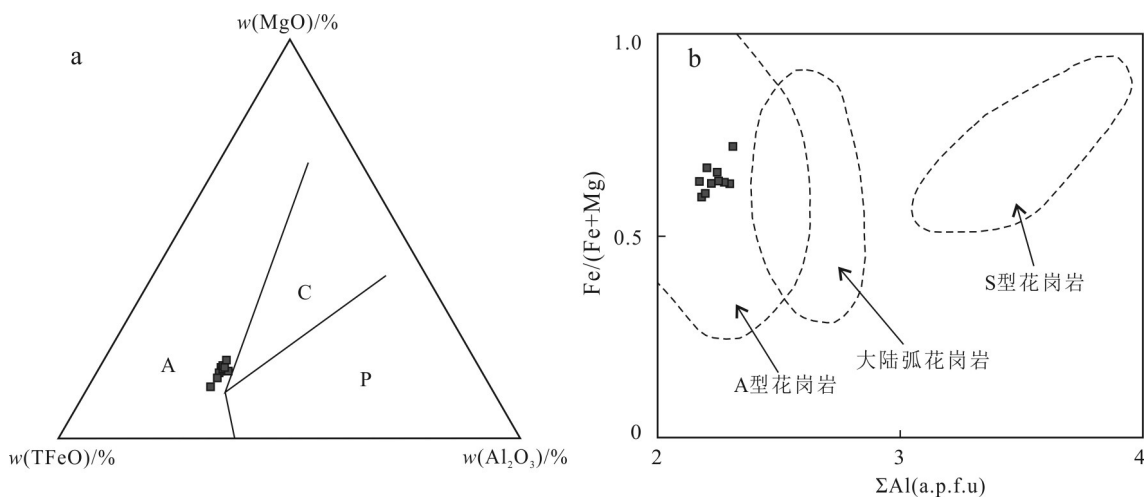


图 10 毛登矿区斑状二长花岗岩黑云母 MgO - TFeO - Al_2O_3 图解(a, 据 Abdel-Rahman, 1994) 和 $\text{Fe}/(\text{Fe}+\text{Mg})$ - ΣAl 图解(b, 据 Shabani et al., 2003)

A—非造山的碱性岩套; C—造山带钙碱性花岗岩; P—过铝质花岗岩

Fig. 10 Plot of MgO - TFeO - Al_2O_3 (a, after Abdel-Rahman, 1994) and $\text{Fe}/(\text{Fe}+\text{Mg})$ - ΣAl (b, after Shabani et al., 2003) of the biotite from the porphyritic monzogranite in the Maodeng deposit

A—Anorogenic alkaline suites; C—Calc-alkaline orogenic suites; P—Peraluminous suites

区阿鲁包格山斑状二长花岗岩为 A 型花岗岩。

4.3.2 岩石源区

姜常义等(1984)研究认为,幔源角闪石 $w(\text{Al}_2\text{O}_3)$ 通常大于 10%,壳源通常小于 10%;幔源角闪石结构式中 $\text{Si}/(\text{Si}+\text{Ti}+\text{Al}) \leq 0.765$,而壳源大于 0.765。本次研究的角闪石属钙质角闪石,角闪石的 $w(\text{Al}_2\text{O}_3)$ 为 5.13%~6.29%, $\text{Si}/(\text{Si}+\text{Ti}+\text{Al})$ 值 0.86~0.88,均显示壳源特征。在角闪石 Al-Si 成因判别图解(图 11)中,毛登样品与浩布高花岗岩中角闪石来源一致,均落入壳源角闪石区域。

黑云母矿物元素组成与岩体元素组成关系密切,可揭示岩浆的源区特征、成因类型以及构造环境(周作侠,1988)。前人研究指出,幔源岩石黑云母通常富镁,壳源岩石黑云母则富铁,且壳源花岗岩的 $I_{\text{Mg}}(\text{Mg}/(\text{Fe}+\text{Mg}))$ 值一般小于 0.5(丁孝石,1988)。本次研究的黑云母富铁($w(\text{TFeO})$ 为 24.73%~28.53%)、贫镁($w(\text{Mg})$ 为 5.67%~8.09%), $I_{\text{Mg}}(0.28\sim 0.39) < 0.5$,显示壳源花岗岩黑云母特征。周作侠(1988)利用 $\text{TFeO}/(\text{TFeO}+\text{MgO})$ - MgO 图解区分不同物质来源的黑云母,图 12 显示斑状二长花岗岩黑云母投点落在壳源花岗岩区域。郭硕等(2019)、李睿华(2019)对毛登矿区斑状二长花岗岩开展岩石地球化学、锆石 Lu-Hf 同位素研究,认为岩体具 A 型花岗岩特征,成岩物质来源于含有大量幔源组分的新生地壳。本

文的角闪石和黑云母矿物学特征指示,斑状二长花岗岩为 A 型花岗岩,成岩物质来源具壳源特征,与前人研究结果一致。

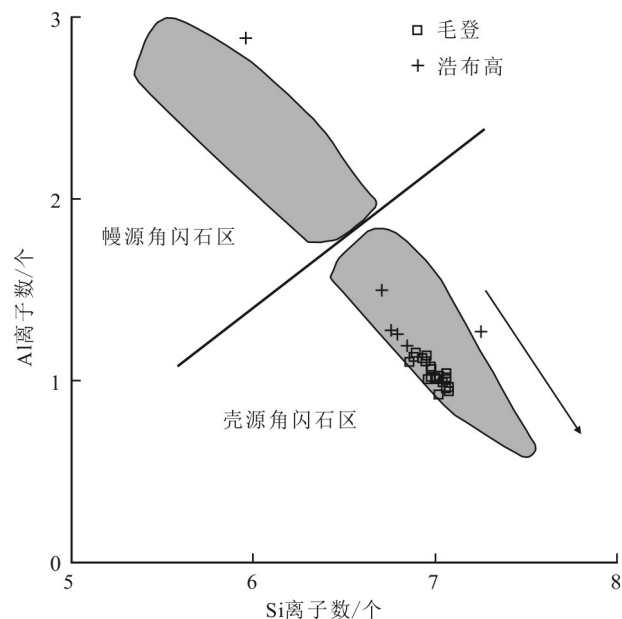


图 11 毛登矿区斑状二长花岗岩角闪石 Al-Si 图解(底图据姜常义等,1984; 数据来源于吕志成等,2003)

Fig. 11 Al-Si diagram of crystal-chemical genesis of amphibole from the porphyritic monzogranite in the Maodeng deposit (base map after Jiang et al., 1984; data after Lü et al., 2003)

4.3.3 构造环境

关于大兴安岭中生代岩浆活动构造背景存在着不同观点,主要包括古太平洋板块俯冲(赵国龙等,1989),蒙古-鄂霍茨克洋闭合后伸展(郭锋等,2001;Fan et al., 2003; Ouyang et al., 2015),古太平洋板块俯冲后撤伸展(王喜龙等,2014;王良玉等,2016),以及蒙古-鄂霍茨克洋造山后伸展和古太平洋板块俯冲联合作用构造背景(张连昌等,2007)。目前,蒙古-鄂霍茨克洋闭合后伸展,或古太平洋板块俯冲后撤伸展构造背景得到较多研究者的支持。

A型花岗岩通常形成于碰撞后(造山后)或板内构造环境,实质上是地壳部分减薄熔融的产物(张旗等,2012)。黑云母Mg-FeO-Al₂O₃和Fe/(Fe+Mg)-ΣAl成因环境判别图解(图10a,b),显示毛登矿区岩体具A型花岗岩特征,形成于拉张构造背景,与前人通过主微量、Lu-Hf同位素(郭硕等,2019;李睿华,2019)、Sr-Nd同位素研究(季根源等,待刊)得到的伸展构造背景结论一致。毛登矿区成岩(矿)时代均为早白垩世,结合区域构造演化史(刘伟等,2007;江思宏等,2018),笔者认为在早白垩世大兴安岭南段毛登地区可能受到蒙古-鄂霍茨克洋造山后伸展和古太平洋俯冲的双重影响,蒙古-鄂霍茨克洋构造域已进入后碰撞阶段,古太平洋板块俯冲方向由N-NNW向NW转变(Engebretson et al., 1985),两大构造域都处于构造体系转变期间,区域构造体系由挤压环境向伸展环境转换过渡

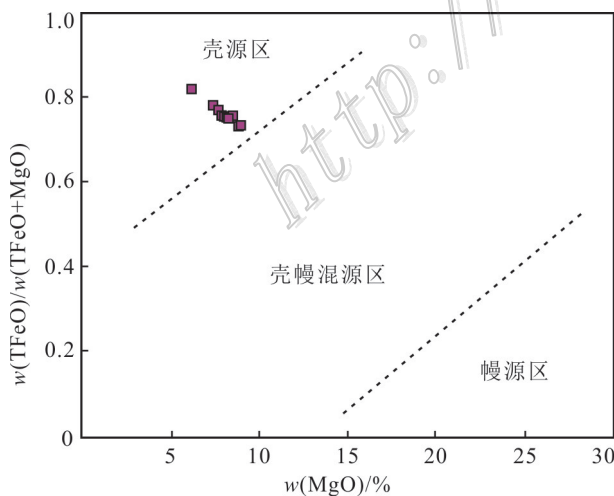


图 12 毛登矿区斑状二长花岗岩黑云母 TFeO/(TFeO+MgO)-MgO 图解(据周作侠,1988)

Fig. 12 Plot of TFeO/(TFeO+MgO)-MgO of the biotite from the porphyritic monzogranite in the Maodeng deposit
(after Zhou, 1988)

期,总体处于伸展构造背景。两大构造体系联合作用也被认为是大兴安岭南段地区燕山晚期成矿高峰期的主要原因(Ouyang et al., 2015;江思宏等,2018)。

4.4 成矿意义

毛登矿床为典型的岩浆热液型矿床,岩浆演化过程中温度、压力、水、卤素逸度等特征制约着后期岩浆热液的形成、演化以及成矿元素沉淀的物理化学条件,是认识成矿过程十分重要的信息。

花岗岩黑云母主量元素组成特征可一定程度上反映寄主岩浆的性质。彭花明(1997)研究认为,华南含锡花岗岩中黑云母的镁质率 $I_{\text{Mg}}(\text{Mg}/(\text{Fe}+\text{Mg}))$ 值为 0.05~0.40;周作侠(1988)研究多种岩体镁铁质云母含铁指数 $I_{\text{Fe}}(\text{Fe}/(\text{Fe}+\text{Mg}))$ 变化对矿化的指示作用,认为在锡、钨、钼成矿关系密切的岩体中 I_{Fe} 值较高,为 0.52~0.92。本次研究的斑状二长花岗岩中黑云母 I_{Mg} 值为 0.28~0.39,位于华南含锡花岗岩 I_{Mg} 值区间范围内; I_{Fe} 值(0.61~0.72)较高,显示斑状二长花岗岩可能为成矿岩体。在不同矿化岩浆岩云母成分图解中,

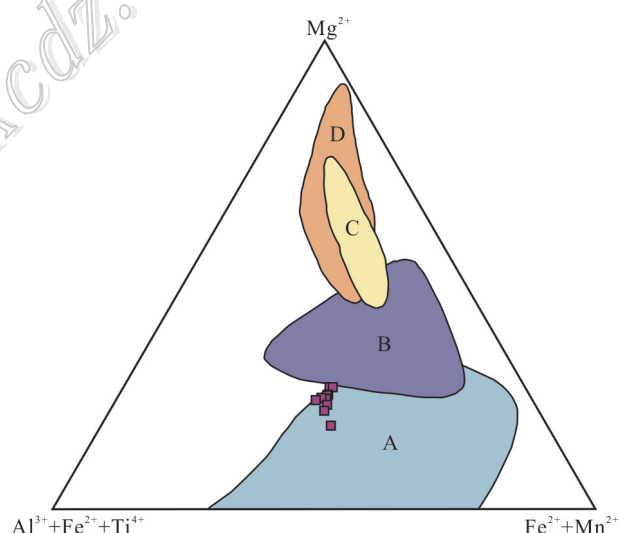


图 13 毛登矿区斑状二长花岗岩黑云母 Mg^{2+} - $(\text{Al}^{3+}+\text{Fe}^{3+}+\text{Ti}^{4+})$ - $(\text{Fe}^{2+}+\text{Mn}^{2+})$ 图解(底图据周云等,2017)

A—锡钨稀土等含矿花岗岩中的铁质黑云母;B—未发现矿化花岗岩中的黑云母;C—与斑岩铜钼矿化有关的镁质黑云母;D—与钒钛磁铁矿及玢岩铁矿有关的镁质黑云母

Fig. 13 Plot of Mg^{2+} - $(\text{Al}^{3+}+\text{Fe}^{3+}+\text{Ti}^{4+})$ - $(\text{Fe}^{2+}+\text{Mn}^{2+})$ of the biotite from the porphyritic monzogranite in the Maodeng deposit (base map after Zhou et al., 1984)

A—Iron biotite in granite containing tin, tungsten and rare earth elements; B—Biotite in unmineralized granite; C—Magnesium biotite associated with porphyry copper-molybdenum mineralization; D—Magnesium biotite associated with vanadium-titanium magnetite or porphyrite iron ore deposit

样品点在锡钨稀土等含矿花岗岩中的铁质黑云母区域(图13)。因此,黑云母矿物元素组成指示了阿鲁包格山岩体与毛登矿区金属成矿作用有密切联系。

全球许多大型-超大型 Sn 矿化作用与花岗岩演化侵入关系密切,而岩浆的氧逸度和温度是制约锡在熔体-流体体系中分配,以及锡富集成矿的主要因素(Linnen et al., 1995; 1996; Stempok, 1990)。Sato (2012)研究认为,W、Sn 矿床与还原性岩浆关系密切,岩浆氧逸度较高时,Sn 以 Sn^{4+} 形式存在,可置换 Ti^{4+} 和 Fe^{3+} 进入岩浆演化早阶段结晶的角闪石、黑云母、磁铁矿等铁镁质矿物,导致残余熔体 Sn 贫化;氧逸度较低时,Sn 以 Sn^{2+} 形式存在,离子半径较大,更趋向在岩浆演化晚阶段的残余熔体-热液中富集(Linnen et al., 1995; 1996),因此,低氧逸度有利于 Sn 富集成矿。Stempok(1990)研究不同温度环境中岩浆 SnO_2 含量变化特征,指出 SnO_2 含量随岩浆结晶时温度的升高而增大。张毓策等(2020)利用个旧锡矿区花岗岩黑云母矿物学特征研究认为,高温、低氧逸度有利于晚期分异的流体形成锡矿床;傅金宝等(1983)研究大厂笼箱盖岩体黑云母矿物学成分认为,黑云母结晶温度约 600°C, 氧逸度 $\lg f(\text{O}_2)$ 约 -17.0, 均有利于锡矿化作用的发育;周云等(2017)对湘东燕山期花岗岩黑云母进行了研究,显示较高温度和较低氧逸度的花岗质岩浆有利于锡富集成矿。本次研究显示,毛登斑状二长花岗岩锆石、角闪石和黑云母晶出时寄主岩浆氧逸度 $\lg f(\text{O}_2)$ 分别为 -16.0、-16.0、-17.5, 温度分别为 734°C、729°C 和 678°C。锆石、角闪石为岩体演化早阶段形成的矿物,黑云母是晚阶段形成的矿物,因此可认为岩浆演化的早-晚阶段均处于较低氧逸度($\lg f(\text{O}_2)$ 为 -19.6~ -14.4)和较高的温度(650~805°C),这有利于锡在熔体中富集。岩浆演化的后期,花岗岩氧逸度随着岩体结晶温度的降低也呈由高到低的变化趋势,锡趋向分配进入成矿流体中,有利于矿区内的大规模成矿。

花岗质岩浆的水含量、卤素逸度条件制约着岩浆热液矿床成矿元素的富集程度。岩浆富水、F 和 Cl 可降低岩浆的固相线温度,促进新生地壳中成矿元素的再活化;其次,流体出溶时间更早,熔体-流体的相互作用时间更长,更有利出溶流体萃取残余熔体中的成矿元素,促进成矿元素的大规模富集;再者,流体出溶,不相容成矿元素优先分配到流体中,F 和 Cl 可影响流体中金属络合物的形成,从而制约成

矿元素的运移和沉淀(张德会等,2001; Robb, 2005; Webster et al., 2009; Sillitoe, 2010; Wang et al., 2014)。岩浆中高含量的 F 元素可促进 Mo 的富集,有利于岩浆晚期流体的出溶分离以及钼矿床形成(Tingle et al., 1984; Scaillet et al., 2004)。如竹溪岭的岩浆体系具高 F 含量、低氧逸度,有利于 Mo 等成矿元素迁移和富集(张振等,2019)。岩浆中 Cl 使 Cu 基本从熔体相中萃取至流体相中,增加出溶流体中 Cu 的含量(Kepper et al., 1991)。成矿流体中高含量的 F 元素利于 Sn 以 $\text{Sn}(\text{OH})_4 \cdot \text{F}_2^{2-}$ 、 $\text{Sn}(\text{OH})\text{F}_3$ 和 Na_2SnF_6 等稳定络合物的形式迁移,伴随温压降低、pH 值升高,锡的氟络合物会发生分解,晶出锡石(Heinrich, 1990; Bhalla et al., 2005)。

本文根据 Ridolfi 等(2008; 2010)提出的角闪石温压计,计算获得岩浆 $\text{H}_2\text{O}_{\text{melt}}$ 为 3.6%~4.4%(平均 4.0%),指示岩浆环境富水。卤素元素在角闪石和黑云母中具有较高的分配系数,因此,角闪石和黑云母矿物中 F、Cl 含量可反映结晶时寄主岩浆中挥发分的富集程度(Latourrette et al., 1995; Lcenhower et al., 1997; 张德会等,2001)。本次研究的角闪石、黑云母成分中 F 和 Cl 含量(表 3、4)均较高,且矿区内的萤石、黄玉等蚀变矿物普遍发育,也暗示了其寄主岩浆富 F 和 Cl。岩浆上升侵位过程中,随着温度、压力的急剧减小,岩浆中富含 H_2O 、Cl、F 等挥发分过饱和,发生流体出溶,形成富集成矿元素的流体。另外,流体包裹体群体成分分析显示,毛登矿区石英-硫化物脉同样富 F 和 Cl 离子(笔者未发表数据),因此,认为毛登矿区成矿流体与岩浆出溶流体性质相同,均富 F 和 Cl,成矿流体来源于岩浆。

随着岩浆的演化,岩浆中 MgO 的含量逐渐降低,TFeO 的含量则逐渐升高,因此,高度结晶分异演化的花岗岩中的角闪石具有较低的 MgO 含量和更高的 TFeO 含量(段登飞等,2017)。斑状二长花岗岩中角闪石的 $w(\text{TFeO})$ 为 22.38%~26.41% (平均 24.36%), $w(\text{MgO})$ 为 5.67%~8.09% (平均 7.16%), 显示富铁、贫镁的特征;在角闪石分类图解(图 6)中,投点落入铁角闪石或铁浅闪石区域,显示富铁特征。前人开展岩体的主、微量元素研究,认为毛登矿区内的斑状二长花岗岩具较高 DI、较低 SI 和强烈 Eu 负异常等特征,也指示了岩浆上升侵位过程经历了明显的结晶分异作用(郭硕等,2019; 李睿华等,2019)。大兴安岭南段地区发育大量与燕山晚期高度演化的花岗岩关系密切的钨、锡、钼、铋、稀土、银等金属矿床,

如白音查干(姚磊等,2017)、维拉斯托(祝新友等,2016)、沙麦(Jiang et al., 2016)、巴尔哲(王一先等,1997; Yang et al., 2014)、小东沟(聂凤军等,2007; 覃峰等,2008; 2009)等。随着花岗质岩浆的分异演化程度增高,其酸性程度增大,硅质、碱值、挥发分和W、Sn、Mo、Bi、REE、稀有等成矿元素在残余花岗质岩浆中逐渐富集,为岩浆活动期后形成钨、锡、钼、铋、稀土、稀有矿床提供物质基础(Jahn et al., 2001; Zhao et al., 2002; Wu et al., 2004)。因此,阿鲁包格山岩体的形成经历了高分异演化作用,为毛登矿区内的锡、钼、铋等金属大规模矿化提供了有利的前提条件。这一研究结果指示,大兴安岭南段地区燕山晚期高度结晶分异演化的花岗岩可作为寻找钨、锡、钼、铋、稀土等金属矿床的找矿标志。

5 结 论

(1) 毛登矿区阿鲁包格山斑状二长花岗岩LA-ICP-MS锆石U-Pb年龄为(140 ± 0.9)Ma,与前人获得的锡石U-Pb等时线年龄(139 ± 3.2)Ma,辉钼矿Re-Os同位素等时线年龄(139 ± 3.9)Ma(笔者未发表数据)在误差范围内近于一致,表明成岩成矿均发生在早白垩世。

(2) 角闪石和黑云母矿物学特征指示,斑状二长花岗岩为A型花岗岩,成岩物质来源具壳源特征;锆石、角闪石和黑云母晶出时寄主岩浆温度分别为 734°C 、 729°C 和 678°C ,氧逸度 $\lg f(\text{O}_2)$ 分别为-16.0、-16.0、-17.5,岩浆水含量为4.0。这些特征表明,斑状二长花岗岩原生岩浆为氧逸度低、水含量高的熔体,随着岩浆的演化,温度逐渐降低,岩浆氧逸度逐渐减小。

(3) 斑状二长花岗岩经历了高度演化作用,具低氧逸度,高温,富水、F、Cl,是毛登矿区锡、钼、铋多金属矿化形成的重要条件。

致 谢 矿物EMPA测试分析工作得到了河北省区域地质矿产调查研究所实验室修迪高级工程师的大力协助,两位评审专家以对本文提出了宝贵的修改意见,在此一并表示衷心的感谢!

References

- Abdel-Rahman A F M. 1994. Nature of biotites from alkaline, calc-alkaline, and peraluminous magmas[J]. *Journal of Petrology*, 35(2): 525-541.
- Anderson J L and Smish D R. 1995. The effects of temperature and $f(\text{O}_2)$ on the Al-in-hornblende barometer[J]. *American Mineralogist*, 80: 549-559.
- Ballard J R, Palin J M and Campbell I H. 2002. Relative oxidation states of magmas inferred from Ce(IV)/Ce(III) in zircon: Application to porphyry copper deposits of northern Chile[J]. *Contributions to Mineralogy and Petrology*, 144(3): 347-364.
- Belousova E A, Griffin W L and O'Reilly S Y. 2006. Zircon crystal morphology, trace element signatures and Hf isotope compositions as a tool for petrogenetic modelling: Examples from eastern Australian granitoids[J]. *Journal of Petrology*, 47(2): 329-353.
- Bhalla P, Holtz F, Linnen R L and Behrens H. 2005. Solubility of cassiterite in evolved granitic melts: Effect of T , $f(\text{O}_2)$, and additional volatiles[J]. *Lithos*, 80(1-4): 387-400.
- Bi X W, Hu R Z, Hanley J J, Mungall J E, Peng J T, Shang L B, Wu K X, Yan S, Li H L and Hu X Y. 2009. Crystallization conditions (T , P , $f(\text{O}_2)$) from mineral chemistry of Cu- and Au-mineralized alkaline intrusions in the Red River-Jinshajiang alkaline igneous belt, western Yunnan Province, China[J]. *Mineralogy and Petrology*, 96(1-2): 43-58.
- Brisken C, Rajaram R, Ayyannan A and Umberto R. 2015. Hydrogen deficiency in Ti-rich biotite from anatexic metapelites (El Joyazo, SE Spain): Crystal-chemical aspects and implications for high-temperature petrogenesis[J]. *American Mineralogist*, 88(4): 583-595.
- Chen Y J, Zhang C, Wang P, Pirajno F and Li N. 2017. The Mo deposits of northeast China: A powerful indicator of tectonic settings and associated evolutionary trends[J]. *Ore Geology Reviews*, 81(2): 602-640.
- Cheng T S, Yang W J and Wang D H. 2014. Zircon U-Pb Age and geochemical characteristics of the Alubaoge A-type granite in Xi-wuqi, Inner Mongolia and its geological significance[J]. *Geotechnica et Metallogenica*, 38(3): 718-728(in Chinese with English abstract).
- Cheng X D, Liu C H, Zhao Y Y, Shui X F, Wang Y C, Gong X, Liu X, Tan W and Xu A M. 2019. Compositional characteristics, petrogenesis and metallogenic significance of amphibole and biotite from Ershiyizhan intrusion in Upper Heilongjiang basin[J]. *Acta Geologica Sinica*, 94(3): 782-798(in Chinese with English abstract).
- Duan D F and Jiang S Y. 2017. The composition of pyroxene and amphibole in ore-related pluton in Jiguanzui Au-Cu skarn deposit, Edong region: Implication for the magma evolution and mineralization[J]. *Acta Petrologica Sinica*, 33(11): 3507-3517(in Chinese with English abstract).
- Elzbieta D, Pawel B, Andrzej K, Wolfgang D, Krzysztof N, Janina S and Cyprian K. 2004. U-Pb dating of serpentinization hydrother-

- mal zircon from a metasomatic rodingite shell(Sudetic ophiolite, SW Poland)[J]. *Chemical Geology*, 203(3): 183-203.
- Engebretson D C, Cox A and Gordon R G. 1985. Relative motions between oceanic and continental plates in the Pacific basin[J]. *Geological Society of America Special Paper*, 206: 1-59.
- Fan W M, Guo F, Wang Y J and Lin G. 2003. Late Mesozoic calcalkaline volcanism of post orogenic extension in the northern Da Hinggan Mountains, northeastern China[J]. *Journal of Volcanology and Geothermal Research*, 121: 115-135.
- Ferry J M and Watson E B. 2007. New thermodynamic models and revised calibrations for the Ti-in-zircon and Zr-in-rutile thermometers[J]. *Contributions to Mineralogy and Petrology*, 154(4): 429-437.
- Foster M D. 1960. Interpretation of the composition of trioctahedral micas[R]. Washington: United States Government Printing Office. 1-49.
- Fu J B, Xu W Y, Zhou W N and Li D M. 1983. Characteristics and geological significance of biotite in Longxiang cover rock of Dachang Tin Mine[J]. *Mineral Deposits*, 3(9): 89-1035(in Chinese with English abstract).
- Gong L, Chen H Y, Xiao B, Wang Y F and Zhao L D. 2018. Mineral chemistry of hornblende in the Chihu-Fuxing copper district, Xinjiang, and its geological significance[J]. *Geochimica*, 47(2): 149-168(in Chinese with English abstract).
- Guo F, Fan Y M, Wang Y J and Lin G. 2001. Petrogenesis of the late Mesozoic bimodal volcanic rocks in the southern Da Hinggan Mts, China[J]. *Acta Petrologica Sinica*, 17(1): 161-168(in Chinese with English abstract).
- Guo S, He P, Zhang X B, Cui Y R, Zhang T F, Zhang K, Lai L and Liu C B. 2019. Geochronology and geochemistry of Maodeng-Xiaogushan tin-polymetallic orefield in southern Da Hinggan Mountains and their geological significances[J]. *Mineral Deposits*, 38(3): 509-525(in Chinese with English abstract).
- Hammarstrom J M and Zen E. 1986. Aluminum in hornblende: An empirical igneous geobarometer[J]. *American Mineralogist*, 71(11-12): 1297-1313.
- Heinrich C A. 1990. The chemistry of hydrothermal Tin-Tungsten ore deposition[J]. *Econ. Geol.*, 85(3): 457-481.
- Henan Provincial Non-ferrous Metal Geological Exploration General Institute. 2019. Detailed investigation report on Mo-Sn-Cu the Maodeng deposit, Xilinhot City, Inner Mongolia[R]. 1-179(in Chinese).
- Henry D J and Guidotti C V. 2003. Titanium in biotite from metapelitic rocks: Temperature effects, crystal-chemical controls and petrologic applications[J]. *American Mineralogist*, 87: 375-382.
- Henry D J, Guidotti C V and Thomson J A. 2005. The Ti-saturationsurface for low-to-medium pressure metapelitic biotites: Implications for geothermometry and Ti-substitution mechanisms[J]. *American Mineralogist*, 90: 316-328.
- Hoskin P W O and Ireland T. 2000. Rare earth element chemistry of zircon and its use as provenance indicator[J]. *Geology*, 28(7): 627-630.
- Hoskin P W O. 2005. Trace-element composition of hydrothermal zircon and the alteration of Hadean zircon from the Jack Hills, Australia[J]. *Geochimica et Cosmochimica Acta*, 69(3): 637-648.
- Hossain I and Tsunigae T. 2014. Crystallization conditions and petrogenesis of the paleoproterozoic basement rocks in Bangladesh: An evaluation of biotite and coexisting amphibole mineral chemistry[J]. *Journal of Earth Science*, 25(1): 87-97.
- Hou K J, Li Y H and Tian Y R. 2009. In situ U-Pb zircon dating using laser ablation-multi ion counting-ICP-MS[J]. *Mineral Deposits*, 28(4): 481-492(in Chinese with English abstract).
- Jahn B M, Wu F Y, Capdevila R, Martineau F, Zhao Z H and Wang Y X. 2001. Highly evolved juvenile granites with tetrad REE patterns: The Woduhe and Baerzhe granites from the Great Xing'an Mountains in NE China[J]. *Lithos*, 59: 171-198.
- Jiang C Y and An S Y. 1984. On chemical characteristics of calcic amphibolies from igneous rocks and their petrogenesis significance[J]. *Journal of Mineralogy and Petrology*, 4(3): 1-9(in Chinese with English abstract).
- Jiang S H, Bagas L, Hu P, Han N, Chen C L, Liu Y and Kang H. 2016. Zircon U-Pb ages and Sr-Nd-Hf isotopes of the highly fractionated granite with tetrad REE patterns in the Shamai tungsten deposit in eastern Inner Mongolia, China: Implications for the timing of mineralization and ore genesis[J]. *Lithos*, 261: 322-339.
- Jiang S H, Zhang L L, Liu Y F, Liu C H, Kang H and Wang F X. 2018. Metallogeny of Xing-Meng orogenic belt and some related problems[J]. *Mineral Deposits*, 37(4): 671-711(in Chinese with English abstract).
- Kang Z Q, Feng Z H and Wang R. 1994. Reliability comparison of Al-in-hornblende and biotite barometer: A case study of Guposhan-Huashan granite in North Guangxi[J]. *Journal of Guilin University of Technology*, 30(4): 474-479(in Chinese with English abstract).
- Kepper H and Wyllie P J. 1991. Partitioning of Cu, Sn, Mo, W, U and Th between melt and aqueous fluid in the system haplogranite H₂O-HCl and haplogranite H₂O-HF[J]. Contribution to Mineralogy and Petrology, 109: 139-150.
- Kumar S and Pathak M. 2010. Mineralogy and geochemistry of biotites from Proterozoic granitoids of western Arunachal Himalaya: Evidence of bimodal granitogenesis and tectonic affinity[J]. *Journal of Geological Society of India*, 75(5): 715-730.
- Latourette T, Hervig R L and Holloway J R. 1995. Trace element partitioning between amphibole, phlogopite, and basanite melt[J]. *Earth and Planetary Science Letters*, 135(1-4): 13-30.
- Leenhouwer J P and London D. 1997. Partitioning of fluorine and chlorine between biotite and granitic melt: Experimental calibration at 200 MPa H₂O[J]. *Contributions to Mineralogy and Petrology*, 127

- (1-2): 17-29.
- Leake B E. 1997. Nomenclature of amphiboles: Report of the subcommittee on amphiboles of the international mineralogical association commission on new minerals and mineral names[J]. Mineralogical Magazine, 61(405): 295-310.
- Li H L, Bi X W, Tu G Z, Hu R Z, Peng J T and Wu K X. 2007. Mineral chemistry of biotite from Yanbei pluton: Implication for Sn-metallageny[J]. Journal of Mineralogy and Petrology, 27(3): 49-54(in Chinese with English abstract).
- Li R H. 2019. Mineralization of tin-copper polymetallic deposits in Xilinhot area of southern Great Xing'an Range(dissertation for Doctor degree)[D]. Supervisor: Wu G. Beijing: Peking University. 1-240(in Chinese with English abstract).
- Li W K, Cheng, Y Q and Yang Z M. 2019. Geo-f(O₂): Integrated software for analysis of magmatic oxygen fugacity[J]. Geochemistry, Geophysics, Geosystems, 20: 2541-2555.
- Lin W W and Peng L J. 1994. The estimation of Fe³⁺ and Fe²⁺ contents in amphibole and biotite from EMPA data[J]. Journal of Changchun University of Earth Sciences, 24(2): 155-162(in Chinese with English abstract).
- Linnen R L, Pichavant M and Holtz F. 1995. The effect of f(O₂) on the solubility, diffusion, and speciation of tin in haplogranitic melt at 850°C and 2 kbar[J]. Geochimica et Cosmochimica Acta, 59(8): 1579-1588.
- Linnen R L, Pichavant M and Holtz F. 1996. The combined effect of f(O₂) and melt composition on SnO₂ solubility and tin diffusivity in haplogranitic melt[J]. Geochimica et cosmochimica acta, 60(24): 4965-4967.
- Liu C H, Wu C L, Lei M, Qin H P and Li M Z. 2013. Petrology and mineralogy of the I-type granites and temperature-pressure conditions for magma formation in the Shahewan Rock mass of the Qinling[J]. Geology and Prospecting, 49(4): 595-608(in Chinese with English abstract).
- Liu J M, Zhang R and Zhang Q Z. 2004. The regional metallogenesis of Da Hinggan Line, China[J]. Earth Science Frontiers, 11(1): 269-273(in Chinese with English abstract).
- Liu R L, Wu G, Li T G, Chen G Z, Wu L W, Zhang P C, Zhang T, Jiang B and Liu W Y. 2018. LA-ICP-MS cassiterite and zircon U-Pb ages of the Weilasituo tin-polymetallic deposit in the southern Great Xing'an Range and their geological significance[J]. Earth Science Frontiers, 25: 1-15(in Chinese with English abstract).
- Liu W, Pan X F, Xie L W and Li H. 2007. Sources of material for the Linxi granitoids, the southern segment of the Da Hinggan Mts: When and how continental crust grew[J]? Acta Petrologica Sinica, 23(2): 441-460(in Chinese with English abstract).
- Liu X L, Li W C, Yin G H and Zhang N. 2013. The geochronology, mineralogy and geochemistry study of the Pulang porphyry copper deposits in Geza arc of Yunnan Province[J]. Acta Petrologica Sinica, 29(9): 3049-3064(in Chinese with English abstract).
- Liu Y F, Jiang S H and Bagas L. 2016. The genesis of metal zonation in the Weilasituo and Bairrendaba Ag-Zn-Pb-Cu-(Sn-W) deposits in the shallow part of a porphyry Sn-W-Rb system, Inner Mongolia, China[J]. Ore Geology Reviews, 75: 150-173.
- Liu Y Q. 1996a. Geology and origin of the Maodeng tin-copper deposit, Inner Mongolia[J]. Mineral deposits, 15(2): 133-143(in Chinese with English abstract).
- Liu Y Q. 1996b. Metallogenic zoning and origin of the Maodeng tin copper deposit[J]. Mineral deposits, 15(4): 318-329(in Chinese with English abstract).
- Liu Y S, Gao S, Hu Z C, Gao S, Gunther D, Xu J, Gao C G and Chen H H. 2008. In situ analysis of major and trace elements of anhydrous minerals by LA-ICP-MS without applying an internal standard[J]. Chemical Geology, 257: 34-43.
- Liu Z, Zhang Y Z, Cui X, Gan C S and Wang Y J. 2020. Petrogenesis and implications of the Late Jurassic granitoid and its mafic microgranular enclaves in West Guangdong Province: Constraints from geochronological, mineralogical and geochemical evidence[J]. Earth Science, 45(4): 1243-1265(in Chinese with English abstract).
- Lü Z C, Duan G Z, Hao L B and Li D C. 2003. Mineral chemistry of amphiboles from granites related to different mineralization and occurred in two stages of Yanshanian period in south-middle part of the Da Xingan mountains and its genetic and metallogenic significance[J]. Journal of Mineralogy and Petrology, 23(1): 5-10(in Chinese with English abstract).
- Ludwig K R. 2003. Isoplot 3.00: A geochronological toolkit for Microsoft Excel[M]. Berkeley Geochronology Center Special Publication. 1-70.
- Luo D, Hou T and Pan R H. 2020. Constraints of oxygen fugacity on the formation of the Panzhihua layered intrusion and its mineralization: Evidence from trace element in zircon[J]. Acta Petrologica Sinica, 36(7): 2116-2126(in Chinese with English abstract).
- Ma X H, Chen B, Lai Y and Lu Y H. 2009. Petrogenesis and mineralization chronology study on the Aolunhua porphyry Mo deposit, Inner Mongolia, and its geological implications[J]. Acta Petrologica Sinica, 25(11): 2939-2950(in Chinese with English abstract).
- Mao J W, Xie G Q, Zhang Z H, Li X F, Wang Y T, Zhang C Q and Li Y F. 2005. Mesozoic large-scale metallogenic pulses in North China and corresponding geodynamic settings[J]. Acta Petrologica Sinica, 21(1): 169-188(in Chinese with English abstract).
- Mao J W, Zhou Z H, Wu G, Jiang S H, Liu C L, Li H M, Ouyang H G and Liu J. 2013. Metallogenic regularity and mineralogenetic series of ore deposits in Inner Mongolia and adjacent areas[J]. Mineral Deposits, 32(4): 715-729(in Chinese with English abstract).
- Nachit H, Ibhi A, Abia E H and Ohoud M B. 2005. Discrimination between primary magmatic biotites, reequilibrated biotites and neofomed biotites[J]. Comptes Rendus Geoscience, 337(16): 1415-1420.

- Nasdala L, Hofmeister W G, Norberg N, Mattinson J M, Corfu F, Dorr W, Kamo S L, Kennedy A K, Kronz A and Reiners P W. 2008. Zircon M257: A homogeneous natural reference material for the ion microprobe U-Pb analysis of zircon[J]. *Geoanalytical Research*, 32: 247-265.
- Nie F J, Zhang W Y, Du A D, Jiang S H and Liu Y. 2007. Re-Os isotopic dating on molybdenite separates from the Xiaodonggou porphyry Mo deposit, Hexigten Qi, Inner Mongolia[J]. *Acta Geologica Sinica*, 81(7): 898-905(in Chinese with English abstract).
- Ouyang H G, Mao J W, Zhou Z H and Su H M. 2015. Late Mesozoic metallogeny and intracontinental magmatism, southern Great Xing'an Range, northeastern China[J]. *Gondwana Research*, 27 (3): 1153-1172.
- Peng H M. 1997. Geological characteristics of biotite from Yangxi granite body and their geological implications[J]. *Acta Petrologica et Mineralogica*, 16(3): 271-281(in Chinese with English abstract).
- Qin F, Liu J M, Zeng Q D and Zhang R B. 2008. The metallogenic epoch and source of ore-forming materials of the Xiaodonggou porphyry molybdenum deposit, Inner Mongolia[J]. *Geoscience*, 22 (2): 173-180(in Chinese with English abstract).
- Qin F, Liu J M, Zeng Q D and Luo Z H. 2009. Petrogenetic and metallogenic mechanism of the Xiaodonggou porphyry molybdenum deposit in Hexigten Banner, Inner Mongolia[J]. *Acta Petrologica Sinica*, 25(12): 3357-3368(in Chinese with English abstract).
- Richards J. 2003. Tectono-magmatic precursors for porphyry Cu-(Mo-Au) deposit formation[J]. *Econ. Geol.*, 98(8): 1515-1533.
- Ridolfi F, Puerini M, Renzulli A, Menna M and Toulkeridis T. 2008. The magmatic feeding system of El Reventador volcano (Sub-Andean zone, Ecuador) constrained by texture, mineralogy and thermobarometry of the 2002 erupted products[J]. *Journal of Volcanology and Geothermal Research*, 176: 94-106.
- Ridolfi F, Renzulli A and Puerini M. 2010. Stability and chemical equilibrium of amphibole in calc-alkaline magmas: An overview, new thermobarometric formulations and application to subduction-related volcanoes[J]. *Contributions to Mineralogy and Petrology*, 160(1): 45-66.
- Robb L. 2005. Introduction to ore forming processes[M]. Oxford: Blackwell Publishing. 1-386.
- Sarjoughian F, Kananian A, Ahmadian J and Murata M. 2015. Chemical composition of biotite from the Kuh-e Dom pluton, Central Iran: Implication for granitoid magmatism and related Cu-Au mineralization[J]. *Arabian Journal of Geosciences*, 8(3): 1521-1533.
- Sato K. 2012. Sedimentary crust and metallogeny of granitoid affinity: Implication from the geotectonic histories of Circun-Japan sea region, Central Andes and southeastern Australia[J]. *Resource Geology*, 62(4): 329-351.
- Scaillet B and Macdonald R. 2004. Fluorite stability in silicic magmas[J]. *Contributions to Mineralogy and Petrology*, 147(3): 319-329.
- Schmidt M W. 1992. Amphibole composition in tonalite as a function of pressure an experimental calibration of the Al-in-Homblende barometer[J]. *Contributions to Mineralogy and Petrology*, 110: 304-310.
- Shabani A A T, Lalonde A E and Whalen J B. 2003. Composition of biotite from granitic rocks of the Canadian Appalachian Orogen: A potential tectonomagmatic indicator[J]? *The Canadian Mineralogist*, 41: 1381-1396.
- Shao J A, Mou B L, Zhu H Z and Zhang L Q. 2010. Material source and tectonic settings of the Mesozoic mineralization of the Da Hinggan Mts[J]. *Acta Petrologica Sinica*, 26(3): 649-656(in Chinese with English abstract).
- Shi D F. 2007. The geological feature and metallogenic model of Maodeng polymetallic ore deposit(dissertation for Master degree)[D]. Supervisor: Zhu Y D. ChangSha: Central South University. 1-72 (in Chinese with English abstract).
- Shu Q H, Chang Z S, Lai Y, Zhou Y T, Sun Y and Yan C. 2016. Regional metallogeny of Mo-bearing deposits in northeastern China, with new Re-Os dates of porphyry Mo deposits in the northern Xilamulun district[J]. *Econ. Geol.*, 111(7): 1783-1798.
- Sillitoe R H. 2010. Porphyry copper systems[J]. *Econ. Geol.*, 105(1): 3-41.
- Spear F S. 1981. Amphibole-plagioclase equilibria: An empirical model for the reaction albite+tremolite=edenite+4 quartz[J]. *Contributions to Mineralogy and Petrology*, 77: 355-364.
- Speer J A. 1984. Micas in igneous rocks[J]. *Reviews in Mineralogy*, 13 (6): 299-356.
- Stemprok M. 1990. Solubility of tin, tungsten and molybdenum oxides in felsic magmas[J]. *Mineralium Deposita*, 25(3): 205-212.
- Stone D. 2000. Temperature and pressure variations in suites of Archean felsic plutonic rocks, Berens River area, northwest Superior Province, Ontario, Canada[J]. *The Canadian Mineralogist*, 38 (2): 455-470.
- Sun S S and McDonough W F. 1989. Chemical and isotopic systematics of oceanic basalts: Implications for mantle composition and processes[A]. In: Saunders A D and Norry M J, eds. *Magmatism in the ocean basins*[C]. Geological Society, London, Special Publications, 42: 313-345.
- Tang P, Tang J X, Zheng W B, Leng Q F and Lin B. 2017. Progress in study of mineral chemistry of magmatic and hydrothermal biotites[J]. *Mineral Deposits*, 36(4): 935-950(in Chinese with English abstract).
- Temizel İ, Arslan M, Abdioğlu E and Yücel C. 2004. Mineral chemistry and thermobarometry of Eocene monzogabbroic stocks from the Bafra (Samsun) area in Turkey: Implications for disequilibrium crystallization and emplacement conditions[J]. *International Geology Review*, 56(10): 1226-1245.
- Tingle T N and Fenn P M. 1984. Transport and concentration of molybdenum in granite molybdenite systems: Effects of fluorine and sulfur[J]. *Geology*, 12(3): 156-158.

- Trail D, Watson F B and Tailby N D. 2012. Ce and Eu anomalies in zircon as proxies for the oxidation state of magmas[J]. *Geochimica et Cosmochimica Acta*, 97: 70-87.
- Wang C M, Zhang S T and Deng J. 2006. The metallogenic space-time structure of copper-polymetallic deposits in the southern segment of Da Hinggan Mountains, China[J]. *Journal of Chengdu University of Technology*, 33(5): 478-484(in Chinese with English abstract).
- Wang F X, Bagas L, Jiang S H and Liu Y F. 2017. Geological, geochemical, and geochronological characteristics of Weilasitu Sn-polymetal deposit, Inner Mongolia, China[J]. *Ore Geology Reviews*, 80: 1206-1229.
- Wang J B, Wang Y W and Wang L J. 2005. Tin-polymetallic metallogenetic series in the southern part of Da Hinggan Mountains, China[J]. *Geology and Prospecting*, 41(6): 15-20(in Chinese with English abstract).
- Wang L Y, Liao Q A, Jiang Y C, Luo T, Hu C B, Xiao D, Tang S and Liu Y. 2016. Petrogenesis and tectonics of Late Early Cretaceous Shoshonitic volcanic rocks in Xilin Hot, Inner Mongolia[J]. *Geological Bulletin of China*, 35(6): 919-931(in Chinese with English abstract).
- Wang R, Richards J P, Hou Z Q, Yang Z M and DuFrane S A. 2014. Increased magmatic water content: The key to Oligo-Miocene porphyry Cu-Mo±Au formation in the eastern Gangdese belt, Tibet[J]. *Econ. Geol.*, 109(5): 1315-1339.
- Wang X L, Liu J J, Zhai D G, Yang Y Q, Wang J P, Zhang Q B and Zhang A L. 2014. U-Pb dating, geochemistry and tectonic implications of Bianjiayuan quartz porphyry, Inner Mongolia, China[J]. *Bulletin of Mineralogy, Petrology and Geochemistry*, 33(5): 654-665(in Chinese with English abstract).
- Wang Y X and Zhao Z H. 1997. Geochemistry and origin of the Baerzhe REE Nb-Be-Zr superlarge deposit[J]. *Geochimical*, 26(1): 24-33(in Chinese with English abstract).
- Wang Y. 2014. The Al-in-hornblende barometry for calc-alkaline igneous rocks: Retrospect, evaluation and applications[J]. *Geological Revies*, 60(4): 839-850(in Chinese with English abstract).
- Webster J D, Sintomi M F and De Vivo B. 2009. The partitioning behavior of Cl, S, and H₂O in aqueous vapor-±saline-liquid saturated phonolitic and trachytic melts at 200 MPa[J]. *Chemical Geology*, 263(1-4): 19-36.
- Wones D R and Eugster H P. 1965. Stability of biotite: Experiment, theory and application[J]. *The American Mineralogist*, 50(9): 1228-1272.
- Wu F Y, Sun D Y, Jahn B M and Wilde S A. 2004. A Jurassic garnet-bearing granitic pluton from NE China showing tetrad REE patterns[J]. *Journal of Asian Earth Sciences*, 23: 731-744.
- Xiang K, Xue C D, Xie Z P and Lai R J. 2019. Petrogenesis of the Late Yanshanian Laba granite in northwestern Yunnan Province and its metallogenetic implications: Evidence from mineral chemistry of biotites and amphiboles[J]. *Acta Petrologica et Mineralogica*, 38(1): 34-46(in Chinese with English abstract).
- Yang W B, Shan Q, Zhao Z H, Luo Y, Yu X Y, Li N B and Niu H C. 2011. Petrogenic and metallogenic action of the alkaline granitoids in Baerzhe Area: A comparison between mineralized and barren plutons[J]. *Journal of Jilin University(Earth Science Edition)*, 41(6): 1689-1704(in Chinese with English abstract).
- Yang W B, Niu H C, Shan, Q, Sun W D, Zhang H, Li N B, Jiang Y H and Yu X Y. 2014. Geochemistry of magmatic and hydrothermal zircon from the highly evolved Baerzhe alkaline granite: Implications for Zr-REE-Nb mineralization[J]. *Mineralium Deposita*, 49: 451-470.
- Yao L, Lü Z C, Ye T Z, Pang Z S, Jia H X, Zhang Z H, Wu Y F and Li R H. 2017. Zircon U-Pb age, geochemical and Nd-Hf isotopic characteristics of quartz porphyry in the Baiyinchagan Sn polymetallic deposit, Inner Mongolia, southern Great Xing'an Range, China[J]. *Acta Petrologica Sinica*, 33(10): 3183-3199(in Chinese with English abstract).
- Ye M, Zhao H, Zhao M, Shu X, Zhang R X and Yang S Y. 2017. Mineral chemistry of biotite and its petrogenesis implication in Lingshan granite pluton, Gan-Hang Belt, SE China[J]. *Acta Petrologica Sinica*, 33(3): 896-906(in Chinese with English abstract).
- Zhai D G, Liu J J, Yang Y Q, Wang J P, Ding L, Liu X W, Zhang M, Yao M J, Su L and Zhang H Y. 2012. Petrogenetic and metallogenetic ages and tectonic setting of the Huanggangliang Fe-Sn deposit, Inner Mongolia[J]. *Acta Petrologica et Mineralogica*, 31(4): 513-523(in Chinese with English abstract).
- Zhai D G, Liu J J, Zhang A L and Sun Y Q. 2017. U-Pb, Re-Os, and ⁴⁰Ar/³⁹Ar geochronology of porphyry Sn±Cu±Mo and polymetallic (Ag-Pb-Zn-Cu) vein mineralization at Bianjiayuan, Inner Mongolia, northeast China: Implications for discrete mineralization events[J]. *Econ. Geol.*, 112: 2041-2059.
- Zhang D H, Zhang W H and Xu G J. 2001. Exsolution and evolution of magmatic hydrothermal fluids and their constraints on the porphyry ore-forming system[J]. *Earth Science Frontiers*, 8(3): 193-202 (in Chinese with English abstract).
- Zhang D H. 2015. Geochemistry of ore-forming processes[M]. Beijing: Geological Press. 1-481(in Chinese).
- Zhang J Q, Li S R and Lu J. 2018. Calculation of oxygen fugacity for intermediate-acidic intrusive rocks[J]. *Acta Mineralogica Sinica*, 38(1): 1-14(in Chinese with English abstract).
- Zhang L C, Chen Z G, Zhou X H, Ying J F, Wang F and Zhang Y T. 2007. Characteristics of deep sources and tectonic-magmatic evolution of the Early Cretaceous volcanics in Genhe area, Da-Hinggan Mountains: Constraints of Sr-Nd-Pb-Hf isotopic geochemistries[J]. *Acta Petrologica Sinica*, 23(11): 2823-2835(in Chinese with English abstract).
- Zhang L L, Jiang S H, Bagas L, Han N, Liu Y and Liu Y F. 2019. Element behaviour during interaction of magma and fluid: A case

- study of Chamuhan granite, and implications on the genesis of W-Mo mineralization[J]. *Lithos*, (342-343): 31-34.
- Zhang Q, Ran H and Li C D. 2012. A-type granite: what is the essence[J]? *Acta Petrologica et Mineralogica*, 31(4): 621-626(in Chinese with English abstract).
- Zhang Q M, Zhai D X and Li H. 2013. Geological characteristics and deposit genesis of Maodeng molybdenum-tin-copper deposit, Inner Mongolia[J]. *Mineral Exploration*, 4(3): 248-256(in Chinese with English abstract).
- Zhang T F, Guo S, Xin H T, Zhang Y, He P, Liu W G, Zhang K, Wang K X and Zhang C. 2019. Petrogenesis and magmatic evolution of highly fractionated granite and their constraints on Sn-(Li-Rb-Nb-Ta) mineralization in the Weilasituo deposit, Inner Mongolia, southern Great Xing'an Range, China[J]. *Earth Science*, 44(1): 248-267(in Chinese with English abstract).
- Zhang X B, Zhou C H, Jia X Q, Wu R Z, Xu C, Yang J, Wang J, Wang M M and Fan C. 2014. LA-ICP-MS zircon U-Pb dating and geochemical characteristics of the porphyroclastic lava in Maodeng area of Inner Mongolia[J]. *Geological Bulletin of China*, 33(7): 974-983(in Chinese with English abstract).
- Zhang X J, Zhang L C, Jin X D, Wu H Y, Xiang P and Chen Z G. 2010. U-Pb ages, geochemical characteristics and their implications of Banlashan molybdenum deposit[J]. *Acta Petrologica Sinica*, 26(5): 1411-1422.
- Zhang Y C, Chen S Y, Zhao J N, Zhao Y H and Li J. 2020. Compositional characteristics and petrogenetic and metallogenetic significance of biotite in granite in Gejiu tin polymetallic ore concentration area, Yunnan Province[J]. *Mineralogy and Petrology*, 40(1): 76-88(in Chinese with English abstract).
- Zhang Z Q, Chen G L, Yang Z K, Tang P, Gao F T, Jiao H J, Wang Z C, Qi J and Wu C N. 2020. Mineral chemistry of biotite and hornblende of ore-bearing porphyry from the Jiamu porphyry copper-polymetallic deposit[J]. *Acta Petrologica et Mineralogica*, 39(6): 685-702(in Chinese with English abstract).
- Zhang Z, Duan X X, Chen B, Wang Z Q, Sun K K and Yan X. 2019. Implications of biotite geochemical characteristics for difference of ore-related magmatic system between Wushan copper deposit and Zhuxiling tungsten deposit[J]. *Acta Petrologica et Mineralogica*, 38(5): 673-692(in Chinese with English abstract).
- Zhao G L, Yang G L, Fu J Y and Yang Y Z. 1989. Mesozoic volcanic rocks in south-middle segment of Da Xinggan Mts[M]. Beijing: Beijing Science and Technology Press. 1-260(in Chinese).
- Zhao Y M and Zhang D Q. 1997. Metallogenetic regularity and prospective evaluation of copper polymetallic deposits in Da Hinggan Mountains and its adjacent regions[M]. Beijing: Earthquake Publishing House. 1-318(in Chinese).
- Zhao Z H, Xiong X L, Han Z D, Wang Y X, Wang Q, Bao Z W and Jahn B M. 2002. Controls on the REE tetrad effect in granites: Evidence from the Qianlishan and Baerzhe granites, China[J]. *Geochemical Journal*, 36: 527-543.
- Zhao Z H. 2010. Trace element geochemistry of accessory minerals and its applications in petrogenesis and metallogenesis[J]. *Earth Science Frontiers*, 17(1): 267-286(in Chinese with English abstract).
- Zhong Y F, Ma C Q and She Z B. 2006. Geochemical characteristics of zircon and its applications in geosciences[J]. *Geological Science and Technology Information*, 25 (1): 27-34(in Chinese with English abstract).
- Zhou Y, Liang X Q, Cai Y F and Fu W. 2017. Petrogenesis and mineralization of Xitian tin-tungsten polymetallic deposit: Constraints from mineral chemistry of biotite from Xitian A-type granite, eastern Hunan Province[J]. *Earth Science*, 42(10): 1647-1657(in Chinese with English abstract).
- Zhou Z H, Lü L S, Yang Y J and Li T. 2010. Petrogenesis of the Early Cretaceous a-type granite in the Huanggang Sn-Fe deposit, Inner Mongolia: Constraints from zircon U-Pb dating and geochemistry[J]. *Acta Petrologica Sinica*, 26(12): 3521-3537(in Chinese with English abstract).
- Zhou Z X. 1988. Chemical characteristics of mafic mica in intrusive rocks and its geological meaning[J]. *Acta Petrologica Sinica*, 3: 63-73(in Chinese with English abstract).
- Zhu X Y, Zhang Z H, Fu X, Li B Y, Wang Y L, Jiao S T and Sun Y L. 2016. Geological and geochemical characteristics of the Weilasituo Sn-Zn deposit, Inner Mongolia[J]. *Geology in China*, 43(1): 188-208(in Chinese with English abstract).
- ### 附中文参考文献
- 程天赦, 杨文静, 王登红. 2014. 内蒙古西乌旗阿鲁包格山A型花岗岩锆石U-Pb年龄、地球化学特征及地质意义[J]. 大地构造与成矿学, 38(3): 718-728.
- 程贤达, 刘春花, 赵元艺, 水新芳, 王远超, 巩鑫, 刘璇, 谭伟, 许安民. 2020. 上黑龙江盆地二十一站岩体角闪石和黑云母成分特征及成岩成矿意义[J]. 地质学报, 94(3): 782-798.
- 段登飞, 蒋少涌. 2017. 鄂东南矿集区鸡冠嘴矽卡岩型金铜矿床含矿岩体中辉石和角闪石成分变化特征及其对岩浆演化和成矿的指示意义[J]. 岩石学报, 33(11): 3507-3517.
- 傅金宝, 许文渊, 周卫宁, 李达明. 1983. 大厂锡矿田龙箱盖岩体黑云母的特征及其地质意义[J]. 矿产与地质, 3(9): 89-103.
- 龚林, 陈华勇, 肖兵, 王云峰, 赵联党. 2018. 新疆赤湖-福兴铜矿区角闪石矿物化学特征及其地质意义[J]. 地球化学, 47(2): 149-168.
- 郭锋, 范蔚茗, 王岳军, 林舸. 2001. 大兴安岭南段晚中生代双峰式火山作用[J]. 岩石学报, 17(1): 161-168.
- 郭硕, 何鹏, 张学斌, 崔玉荣, 张天福, 张阔, 来林, 刘传宝. 2019. 大兴安岭南段毛登-小孤山锡多金属矿田年代学、地球化学特征及其地质意义[J]. 矿床地质, 38(3): 509-525.
- 河南省有色金属地质勘查总院. 2009. 内蒙古自治区锡林浩特市毛登矿区钼锡铜矿详查报告[R]. 1-179.

- 侯可军,李延河,田有荣. 2009. LA-MC-ICP-MS 锆石微区原位 U-Pb 定年技术[J]. 矿床地质,28(4):481-492.
- 江思宏,张莉莉,刘翼飞,刘春花,康欢,王丰翔. 2018. 兴蒙造山带成矿规律及若干科学问题[J]. 矿床地质,37(4):671-711.
- 姜常义,安三元. 1984. 论火成岩中钙质角闪石的化学组成特征及其岩石学意义[J]. 矿物岩石,4(3):1-9.
- 康志强,冯佐海,王睿. 1994. 角闪石黑云母全铝压力计的可靠性对比——以广西姑婆山-花山花岗岩为例[J]. 桂林理工大学学报,30(4):474-479.
- 李鸿莉,毕献武,涂光炽,胡瑞忠,彭建堂,吴开兴. 2007. 岩背花岗岩黑云母矿物化学研究及其对成矿意义的指示[J]. 矿物岩石,27(3):49-54.
- 李睿华. 2019. 大兴安岭南段锡林浩特地区锡铜多金属矿床的成矿作用(博士学位论文)[D]. 导师:武广. 北京:北京大学. 1-240.
- 林文蔚,彭丽君. 1994. 由电子探针分析数据估算角闪石、黑云母中的 $\text{Fe}^{3+}/\text{Fe}^{2+}$ [J]. 长春地质学院学报,24(2):155-162.
- 刘春花,吴才来,雷敏,秦海鹏,李名则. 2013. 秦岭沙河湾 I型花岗岩岩石学、矿物学特征及岩浆形成的温压条件[J]. 地质与勘探,49(4):595-608.
- 刘建明,张锐,张庆洲. 2004. 大兴安岭地区的区域成矿特征[J]. 地学前缘,11(1):269-273.
- 刘瑞麟,武广,李铁刚,陈公正,武利文,章培春,张彤,江彪,刘文元. 2018. 大兴安岭南段维拉斯托基多金属矿床 LA-ICP-MS 锆石和锆石 U-Pb 年龄及其地质意义[J]. 地学前缘,25:1-15.
- 刘伟,潘小菲,谢烈文,李禾. 2007. 大兴安岭南段林西地区花岗岩类的源岩:地壳生长的时代和方式[J]. 岩石学报,23(2):441-460.
- 刘学龙,李文昌,尹光候,张娜. 2013. 云南格咱岛弧普朗斑岩型铜矿年代学、岩石矿物学及地球化学研究[J]. 岩石学报,29(9):3049-3064.
- 刘玉强. 1996a. 内蒙古毛登锡铜矿床地质及成因[J]. 矿床地质,15(2):133-143.
- 刘玉强. 1996b. 毛登锡铜矿床成矿分带及其成因讨论[J]. 矿床地质,15(4):318-329.
- 刘梓,张玉芝,崔翔,甘成势,王岳军. 2020. 粤西晚侏罗世花岗岩质体及其暗色微粒包体的成因及意义:年代学、矿物学和地球化学约束[J]. 地球科学,45(4):1243-1265.
- 罗雕,侯通,潘荣昊. 2020. 氧逸度对攀枝花岩体成岩成矿作用的制约:来自锆石微量元素的证据[J]. 岩石学报,36(7):2116-2126.
- 吕志成,段国正,郝立波,李殿超. 2003. 大兴安岭中南段燕山期两类不同成矿花岗岩类角闪石的化学成分及其成岩成矿意义[J]. 矿物岩石,23(1):5-10.
- 马星华,陈斌,赖勇,鲁颖淮. 2009. 内蒙古敖伦花斑岩铜矿床成岩成矿年代学及地质意义[J]. 岩石学报,25(11):2939-2950.
- 毛景文,谢桂青,张作衡,李晓峰,王义天,张长青,李永峰. 2005. 中国北方中生代大规模成矿作用的期次及其地球动力学背景[J]. 岩石学报,21(1):169-188.
- 毛景文,周振华,武广,江思宏,刘成林,李厚民,欧阳荷根,刘军. 2013. 内蒙古及邻区矿床成矿规律与成矿系列[J]. 矿床地质,32(4):715-729.
- 聂凤军,张万益,杜安道,江思宏,刘妍. 2007. 内蒙古小东沟斑岩型钼矿床辉钼矿铼-锇同位素年龄及地质意义[J]. 地质学报,81(7):898-905.
- 彭光明. 1997. 杨溪岩体中黑云母的特征及其地质意义[J]. 岩石矿物学杂志,16(3):271-281.
- 邵济安,牟保磊,朱慧忠,张履桥. 2010. 大兴安岭中南段中生代成矿物质的深部来源与背景[J]. 岩石学报,26(3):649-656.
- 石得风. 2007. 内蒙古锡林浩特市毛登多金属矿区地质特征及成矿模式研究(硕士学位论文)[D]. 导师:朱余德. 长沙:中南大学. 1-72.
- 覃锋,刘建明,曾庆栋,张瑞斌. 2008. 内蒙古小东沟斑岩型钼矿床的成矿时代及成矿物质来源[J]. 现代地质,22(2):173-180.
- 覃锋,刘建明,曾庆栋,罗照华. 2009. 内蒙古克什克腾旗小东沟斑岩型钼矿床成岩成矿机制探讨[J]. 岩石学报,25(12):3357-3368.
- 唐攀,唐菊兴,郑文宝,冷秋锋,林彬. 2017. 岩浆黑云母和热液黑云母矿物化学研究进展[J]. 矿床地质,36(4):935-950.
- 汪洋. 2014. 钙碱性火成岩的角闪石全铝压力计——回顾、评价和应用实例[J]. 地质论评,60(4):839-850.
- 王京彬,王玉往,王莉娟. 2005. 大兴安岭南段锡多金属成矿系列[J]. 地质与勘探,41(6):15-20.
- 王良玉,廖群安,江云川,罗婷,胡朝斌,肖典,汤帅,刘洋. 2016. 内蒙古锡林浩特早白垩世晚期钾玄质火山岩成因及构造环境[J]. 地质通报,35(6):919-931.
- 王喜龙,刘家军,翟德高,杨永强,王建平,张琪彬,张安立. 2014. 内蒙古边家大院矿区石英斑岩 U-Pb 年代学、岩石地球化学特征及其地质意义[J]. 矿物岩石地球化学通报,33(5):654-665.
- 王一先,赵振华. 1997. 巴尔哲超大型稀土铌铍锆矿床地球化学和成因[J]. 地球化学,26(1):24-33.
- 王长明,张寿庭,邓军. 2006. 大兴安岭南段铜多金属成矿时空结构[J]. 成都理工大学学报(自然科学版),33(5):478-484.
- 向坤,薛传东,谢志鹏,来瑞娟. 2019. 滇西北拉巴燕山晚期花岗岩岩石成因及其成矿指示——黑云母和角闪石矿物化学证据[J]. 岩石矿物学杂志,38(1):34-46.
- 杨武斌,单强,赵振华,罗勇,于学元,李宁波,牛贺才. 2011. 巴尔哲地区碱性花岗岩的成岩和成矿作用:矿化和未矿化岩体的比较[J]. 吉林大学学报(地球科学版),41(6):1689-1704.
- 姚磊,吕志成,叶天竺,庞振山,贾宏翔,张志辉,吴云峰,李睿华. 2017. 大兴安岭南段内蒙古白音查干 Sn 多金属矿床石英斑岩的锆石 U-Pb 年龄、地球化学和 Nd-Hf 同位素特征及地质意义[J]. 岩石学报,33(10):3183-3199.
- 叶茂,赵赫,赵沔,舒珣,张若曦,杨水源. 2017. 赣杭构造带灵山花岗岩体黑云母的矿物化学特征及其对岩石成因的指示意义[J]. 岩石学报,33(3):896-906.
- 翟德高,刘家军,杨永强,王建平,定立,刘星旺,张梅,要梅娟,苏犁,张红雨. 2012. 内蒙古黄岗梁铁锡矿床成岩、成矿时代与构造背景[J]. 岩石矿物学杂志,31(4):513-523.
- 张德会,张文淮,许国建. 2001. 岩浆热液出溶和演化对斑岩成矿系统金属成矿的制约[J]. 地学前缘,8(3):193-202.
- 张德会. 2015. 成矿作用地球化学[M]. 北京:地质出版社. 1-481.

- 张聚全,李胜荣,卢静. 2018. 中酸性侵入岩的氧逸度计算[J]. 矿物学报,38(1):1-14.
- 张连昌,陈志广,周新华,英基丰,王非,张玉涛. 2007. 大兴安岭根河地区早白垩世火山岩深部源区与构造-岩浆演化: Sr-Nd-Pb-Hf 同位素地球化学制约[J]. 岩石学报,23(11):2823-2835.
- 张旗,冉皞,李承东. 2012. A型花岗岩的实质是什么[J]? 岩石矿物学杂志,31(4):621-626.
- 张巧梅,翟东兴,李华. 2013. 内蒙古毛登钼锡铜矿床地质特征及成因探讨[J]. 矿产勘查,4(3):248-256.
- 张天福,郭硕,辛后田,张云,何鹏,刘文刚,张阔,王可祥,张超. 2018. 大兴安岭南段维拉斯托高分异花岗岩体的成因与演化及其对 Sn-(Li-Rb-Nb-Ta)多金属成矿作用的制约[J]. 地球科学,246:3521-3537.
- 张学斌,周长红,贾晓青,吴荣泽,徐翠,杨菊,王明明,范超. 2014. 内蒙古毛登地区碎斑熔岩 LA-ICP-MS 锆石 U-Pb 年龄与地球化学特征[J]. 地质通报,33(7):974-983.
- 张毓策,陈守余,赵江南,赵月华,李姜. 2020. 云南个旧锡多金属矿区花岗岩中黑云母的成分特征及成岩成矿意义[J]. 矿物岩石,40(1):76-88.
- 张振,殷晓侠,陈斌,王志强,孙克克,严翔. 2019. 黑云母地球化学特征对武山铜矿和竹溪岭钨矿成矿岩浆体系差异的指示[J]. 岩石矿物学杂志,38(5):673-692.
- 张忠坤,陈国良,杨征坤,唐攀,高福太,焦海军,王志超,祁婧,吴纯能. 2020. 西藏甲玛铜多金属矿含矿斑岩黑云母和角闪石矿物化学特征[J]. 岩石矿物学杂志,39(6):685-702.
- 赵国龙,杨桂林,傅嘉友,杨玉琢. 1989. 大兴安岭中南部中生代火山岩[M]. 北京:北京科学技术出版社. 1-260.
- 赵一鸣,张德全. 1997. 大兴安岭及其邻区铜多金属矿床成矿规律与远景评价[M]. 北京:地震出版社. 1-318.
- 赵振华. 2010. 副矿物微量元素地球化学特征在成岩成矿作用研究中的应用[J]. 地学前缘,17(1):267-286.
- 钟玉芳,马昌前,余振兵. 2006. 锆石地球化学特征及地质应用研究综述[J]. 地质科技情报,25 (1):27-34.
- 周云,梁新权,蔡永丰,付伟. 2017. 湘东锡田燕山期 A型花岗岩黑云母矿物化学特征及其成岩成矿意义[J]. 地球科学,42(10):1647-1657.
- 周振华,吕林素,杨永军,李涛. 2010. 内蒙古黄岗锡铁矿区早白垩世 A型花岗岩成因: 锆石 U-Pb 年代学和岩石地球化学制约[J]. 岩石学报,26(12):3521-3537.
- 周作侠. 1988. 侵入岩的镁铁云母化学成分特征及其地质意义[J]. 岩石学报,3:63-73.
- 祝新友,张志辉,付旭,李柏阳,王艳丽,焦守涛,孙雅琳. 2016. 内蒙古赤峰维拉斯托大型锡多金属矿的地质地球化学特征[J]. 中国地质,43(1):188-208.